we calculate maximum magnitudes as if they were separate faults with aspect ratios consistent with their lengths. (Further discussion in sections on maximum magnitudes and synchronous rupture). Alternative dips and aspect ratios are considered for Yucca Mountain faults in the assessment of their downdip extent.

(4) Given the local faults may have merging geometries, for multi-fault-rupture scenarios we compute the fault area as the sum of areas for all faults that ruptured. Note, however, that unless the separate faults ruptured simultaneously (i.e., within about 30 seconds of each other in our definition), we interpret that these scenario earthquakes to be separate earthquakes spaced a few hours to decades apart, with correspondingly lower magnitudes than a large simultaneous rupture.

(5) Fault slip is dominantly dip slip in the northern part of the area; southward, the horizontal component increases via vertical axis rotation. It is not known whether this is due to a local effect at the southeast edge of Crater Flat, or to a subordinate tectonic rotation induced by a right-lateral fault zone in Amargosa Valley.

In addition to the above, our model must include the following elements from the Detachment and Lateral Shear Models:

(6) The possibility of a deep detachment (>6 km) cannot be ruled out by the existing geophysics. Therefore, we allow some probability to the existence of such a detachment (P=0.15) and an even lower weight to it being seismogenic. The likelihood that faults merge at depth is dependent, in part, on the depth of the inferred detachment.

(7) The oblique component of slip on Yucca Mountain faults and the clockwise vertical axis rotation are related to dextral strain (bending) transmitted from the Walker Lane. However, it is unclear whether discrete northwest-striking dextral faults exist north and south of Yucca Mountain (defining a rhombochasm), or whether lateral strain is diffuse. This model utilizes recognized faults as the eastern and western margins of the rhombochasm (Bare Mountain fault, Paintbrush Canyon/Stagecoach Road fault) and an inferred fault (Carrara feature) as the southern margin. These three faults are already characterized on the SSC logic tree, so no further additions to the logic tree are required for this tectonic model. The northern margin of the rhombochasm is approximately coincident with the Yucca Wash fault, to which we assign a 0% probability of being seismogenic, based on its lack of evidence for Quaternary displacement.

(8) The probability that a buried, strike-slip fault exists is dependent on the probability of a detachment. If a detachment fault exists (probability = 15%), then we consider that there is a 20% probability that a buried strike-slip fault exists (net probability = 3%). If no detachment exists (probability = 85%), then there is only a 5% chance that the buried strike-slip fault exists (net probability = 4%). The sum of the two net probabilities that the buried fault exists is thus 7%. The probability that the buried strike-slip fault is seismogenic is dependent on the depth of the detachment.

Although a volcano-tectonic source is not explicitly included as a separate source model, we include one element from the Volcanic-Tectonic Model. This element does not require a caldera source, but depends on the simultaneous basaltic volcanic eruption and the extensive tectonic, seismogenic rupturing of several faults that extend northward from a Lathrop Cone volcanic source. The possibility of such a scenario is accounted for in the simultaneous rupture portion of the local fault model.

(1) Some surface-rupturing paleoearthquakes (e.g., Scenario U) probably have accompanied episodes of basalt eruption and dike injection.

(2) Although there may be some volcanic-tectonic connection, the possibility of volcanic earthquakes does not affect our estimates of earthquake magnitude and recurrence. Therefore, we do not include a separate volcanic earthquake branch on our seismic source characterization logic tree, for two reasons. First, the maximum magnitude of volcanic earthquakes associated with dike injection (M = 5.5) and calderas (M = 4.5± 1.2) (Hackett *et al.*, 1996) are much smaller than our estimated maximum magnitudes for tectonic earthquakes, either on individual faults or for background seismic zones. Second, the recurrence interval of volcanic eruptive events is estimated to be ca. 200 to 300 ka by the experts in volcanic hazards assessment for Yucca Mountain. Thus, any volcanic contribution to earthquake hazard is insignificant compared to the rates of background seismicity in and near Yucca Mountain (see Section 3.6).

Behavioral aspects such as distributed, multi-fault earthquakes, could occur in any of the tectonic models. However, simultaneous faulting on parallel normal faults may be more easily explained by the Volcanic-Tectonic Model (which we have not included as a separate source model) than by the Lateral Shear Model (a variant of which we weight at 20%), and least by the Planar Block Model (which we give the highest weight at 80%). Thus, our

weighting of tectonic models reflects our interpretation that simultaneous multi-fault ruptures (i.e., within a ~30- second time span) have a low probability.

3.0 SEISMIC SOURCES

The characterization of fault-specific sources in the Yucca Mountain region is based on our preferred tectonic model as summarized on Figure ASM-1. In addition to these fault sources, our seismic source model also includes more regional faults (i.e., those outside the immediate vicinity of Yucca Mountain/Crater Flat) and areal source zones.

The seismogenic potential of potential sources in the Yucca Mountain region is partly a function of the depth of the brittle (seismogenic) crust. Therefore, we first consider the assessment of the thickness of the seismogenic crust.

3.1 THICKNESS OF THE SEISMOGENIC CRUST

The depth of the brittle/seismogenic crust is assessed to be 12 km (0.1), 15 km (0.6), and 17 km (0.3). These depths and their relative weights are based on the distribution of focal depths for instrumental earthquakes in the southern Great Basin, as given in von Seggern and Brune (1997), and Harmsen and Bufe (1991), the focal depths in the Yucca Mountain region summarized by K. Smith at SSC Workshop 2, and discussions presented by Robert Smith at SSC Workshop 5. The nucleation depths of $M > 6$ earthquakes in the Basin and Range province in general (Rogers *et al.*, 1991), and in southwestern Nevada in particular (e.g., the Little Skull Mountain earthquake; Smith *et al.*, 1997) are near the base of the seismogenic crust. This fact will be important in evaluating the existence of detachments deep in the crust.

3.2 DETACHMENT AS SEISMIC SOURCE

For this analysis, a detachment fault is defined as a regionally extensive, low-angle (< 15-20 degree) surface that truncates high-angle faults and lies within the brittle crust. A detachment would lie within the upper 6 to 15 km of the crust. A subhorizontal surface lying beneath the

brittle-ductile transition would not be considered a detachment within this terminology. The assessment of a detachment as a seismic source will evaluate seismogenic potential, depth of the structure, geometry, maximum magnitude and recurrence. Figure ASM-2 contains the logic tree detailing our assessment of this source.

3.2.1 Seismogenic Potential

The seismogenic potential for a detachment is judged to be a function of its existence, geometry and extent. This dependency is shown in the following logic tree (Figure ASM-2).

The first assessment is whether a detachment exists. The weight assigned to the existence of a detachment is 0.15 and to no detachment is 0.85. The following evidence supports the existence of a detachment: a detachment would explain the many narrow, parallel fault blocks as dominos above a detachment; Tertiary detachment faults exist in the region surrounding Yucca Mountain; and normal faults may utilize parts of old detachments, such as those in the Overthrust Belt (Smith and Arabasz, 1992; Arabasz *et al.*, 1992). The arguments against a detachment are: a lack of evidence for low-angle faulting from the seismicity, including the Little Skull Mountain earthquake; the known detachments east and west of Yucca Mountain are old (> 6 Ma); basaltic volcanism requires deep penetrating structures; elsewhere in the region, there is no detachment at the Tertiary/Paleozoic boundary; movement on the Bare Mountain fault would have truncated the detachment; and, a deep detachment could not produce the observed dip rollovers and opposed slip on some faults (C. Fridrich, SSC Workshop 3).

The second assessment is the depth of the detachment, conditional on its existence. Three depths are considered, which depend on the depth of the brittle crust. The minimum depth is 6 km, which is below the depth observed in the seismic reflection profile presented by T. Brocher (SSC Workshop 2). There is no evidence for a low-angle detachment fault on the seismic reflection profile, although such a structure should have been obvious if it existed. Therefore, if a detachment fault exists beneath Crater Flat, it must lie at or below 6 km. The maximum depth for a detachment beneath Crater Flat is the depth of the brittle-ductile transition (which, as discussed above, is assumed to lie between 12 and 17 km depth). An intermediate depth of the detachment is considered, halfway between the depth of the brittle-ductile transition and 6 km. This would place the detachment toward the base of the

seismogenic crust, which is the most common nucleation point for large earthquakes in the region (Rogers *et al.*, 1991). The relative weights assigned to the three alternative depths are 6 km (0.25), (BD-6)/2 + 6 (0.5), and BD (0.25), where BD is the depth of the brittle-ductile transition. The weights assigned to the three interpretations are based on the following observations: (1) A shallow depth for the detachment conflicts with the geometry of the Bare Mountain fault. The Bare Mountain fault would be truncated at a shallow depth that is a significant fraction of the total offset on the fault; lack of analogs to this situation suggest a low weight for this interpretation. (2) The observed opposed dips on some of the Crater Flat faults are inconsistent with normal faulting caused by extension above a subjacent detachment. This scenario also receives a low weight.

- The next conditional assessment is whether the detachment is seismogenic, that is, capable of generating significant ($M > 5$) earthquakes in the present tectonic regime. This assessment is independent of the depth of the detachment. The possibility that a detachment (if it exists) is seismogenic is given a very low weight (0.01) based on both theoretical reasoning and empirical data. First, according to Mohr-Coulomb theory of brittle failure, given a horizontal least-principal stress and rocks having internal friction angles of 30 ± 10 degrees, the most likely dip for active normal faults is 60 ± 10 degrees (see extended discussion by Sibson, 1985). A fault dipping only 10 to 20 degrees would be in a very unfavorable orientation for slip, compared to the multitude of faults having dips closer to 60 degrees at Yucca Mountain. [Forsyth (1992) rebuts this argument, saying that if the low-angle fault had sufficiently lower strength than the high-angle faults, slip might be accommodated.] These higher-angle faults have demonstrated Quaternary slip, proving that they have accommodated Quaternary extension, as would be predicted by theory. The existence of a low-angle detachment beneath Crater Flat is merely conjectural; there is no evidence that it exists, much less that it has accommodated any Quaternary slip.

Second, although low-angle detachments have been widely described in the southwest United States (e.g., Wernicke, 1995), even after 15 years of research only one of these detachments shows evidence of Quaternary activity. The sole exception (Johnson and Loy, 1992) is a case where Quaternary fault scarps exist on the trace of the Santa Rita (Arizona) fault, which has a dip determined from seismic reflection data of 19 degrees to a depth of at least 6 km. To our knowledge this is the only documented instance of Quaternary fault scarps overlying a

low-angle normal fault; although in other areas (e.g., the Overthrust Belt of Wyoming) Quaternary fault scarps commonly overlie faults interpreted as having listric geometry (McCalpin, 1991).

Third, published summaries of focal mechanisms of earthquakes in extensional regimes show few or no cases of seismogenic rupture on low-angle normal faults (Jackson, 1987; Jackson and White, 1989; Doser and Smith, 1989; Wernicke, 1995). We estimate that there are several hundred documented focal mechanisms of significant ($M > 4$) normal-faulting earthquakes worldwide. Only two of those events (the Papua New Guinea earthquake [Abers, 1991], and the 1946 Ancash, Peru earthquake [Doser, 1987]) appear to have possibly occurred on low-angle faults. [As in any double-couple energy release, inversion for a focal mechanism can only resolve two nodal planes, one of which is the true nodal plane]. The interpretation of the true nodal plane in the New Guinea event is equivocal, and the Ancash event probably occurred on a reactivated thrust. Thus, despite the acknowledged existence of low-angle detachment faults in many extensional terranes, there are only two instances of those faults possibly generating earthquakes, compared to hundreds of instances of high-angle normal faults generating earthquakes. In the Yucca Mountain region, the historical record shows earthquakes only on higher-angle faults (e.g., the Little Skull Mountain earthquake and focal mechanism compilations of Gomberg *et al.*, 1991a; Rogers *et al.*, 1991).

Based on the scarcity (or absence) of earthquakes generated by detachment faults, we weight the probability that a sub-Yucca Mountain detachment is seismogenic as 0.01. The possibility for a seismogenic detachment is included in the analysis, despite its very low weight, to allow for the slight chance that the hypothesis proposed by Wernicke (1995) might apply to the Yucca Mountain region. Wernicke proposes that the paucity of earthquakes on low-angle normal faults is caused by long recurrence intervals on this type of fault, compared to recurrence intervals on high-angle normal faults that have the same strain rate. Given the short period for which we have reliable focal mechanism data (roughly since 1960), Wernicke (1995) argued that the period of observation is too short to capture many earthquakes on detachments that have very long recurrence intervals.

Hypotheses that claim the period of observation is too short to capture a particular observation usually are tested through the ergodic substitution of space for time (Hunter and Mann, 1995). However, in this case we are already analyzing a worldwide data set, so expanding the area over which data were collected is not possible. Given that Wernicke's (1995) hypothesis is not directly testable, but claims very large earthquake magnitudes for long-recurrence detachment faults, we decided to assign a nonzero (but small) probability for the seismic potential of a sub-Yucca Mountain detachment fault.

3.2.2 Geometry

Typical dimensions of detachment faults elsewhere in the world (summarized by Wernicke, 1995, p. 20,170) are: strike lengths of 60 to 180 km and downdip lengths of 60 to 70 km. Based on these dimensions, a detachment, if it were to exist, would underlie the entire Crater Flat/Yucca Mountain region, which is only about 20 x 20 km. The break-away for the detachment (its eastern extent) would be in the middle of Jackass Flat and would extend beneath Bare Mountain on the west. By analogy to the Bullfrog Hills (the nearest detachment fault to the site), and to the typical dips of detachment faults cited by Wernicke (1995), the detachment is assumed to dip 15 to 20 degrees to the west. The north-south extent of the detachment underlying the Crater Flat region is assumed to be the same as the extent of the north-south normal faults. This extent (about 25 km) is considerably smaller than that cited by Wernicke. Our reasoning is as follows. First, if the north-south-trending normal faults around Crater Flat are the surface expressions of an underlying detachment, then the detachment should not extend far beyond that surface expression. It is possible that the Timber Mountain caldera north of Crater Flat, and the Walker Lane south of Crater Flat, could somewhat obscure this structural relationship. Thus, the north-south extent of normal faults near Yucca Mountain (25 km; probability 0.25) sets a minimum along-strike distance for a detachment, with a preferred value of 60 km (0.5) and a maximum value of 120 km (probability 0.25). Downdip extent (based on a dip of 10 to 20 degrees and a crustal thickness of 12 to 17 km; all values equally likely) ranges from 35 km (probability 0.25) to 48 km (0.25), 69 km (0.25), or 98 km (0.25). The resulting area of the hypothesized detachment thus would average about 4000 km^2, with a standard deviation of about 2000 km^2.

3.2.3 Maximum Magnitude

The maximum magnitude of a detachment-fault earthquake would arise from rupture of the entire 4000 ± 2000 km^2 surface area estimated for the detachment. A rupture of this dimension, using the empirical relationship between rupture area and magnitude for all slip types of Wells and Coppersmith (1994) results in a mean estimated earthquake magnitude of 7.6 (+0.2, -0.3). Adding the uncertainty from the Wells and Coppersmith (1994) empirical regression (0.24 magnitude unit), our estimated magnitude for the maximum detachment earthquake is 7.6 (+ 0.4, -0.5) at a 1-sigma range. We assign weights of 0.15, 0.7, and 0.15 to these values.

3.2.4 Recurrence

Because of the absence of earthquakes having low-angle focal mechanisms in the historical record in this area, it is impossible to associate earthquakes with a detachment and use the rate of those events to constrain recurrence rates. A method for constraining recurrence is to resolve the Quaternary slip rates (using the weights arrived at for the those values as discussed in a later section) of all Yucca Mountain faults along three equally spaced east-west transects. We use the same transects as shown in L. Anderson's presentation at SSC Workshop 3. We then consider the largest of those three values to be equal to the slip rate of the detachment. Our reasoning is thus: If the surface faults are expressions of extension on the underlying detachment, their combined slip rate cannot be greater than the slip rate on the detachment. However, the combined surface slip rate could be smaller than that on the detachment, if there is any component of nonelastic deformation above the detachment, or if there is any elastic deformation on faults that do not reach the surface. Therefore, the surface slip rate is a minimum value for the detachment slip rate.

The results are:
Slip Rate = 0.05 mm/yr; Probability = 0.6
Slip Rate = 0.013 mm/yr; Probability = 0.2
Slip Rate = 0.12 mm/yr; Probability = 0.2

Displacement per event is calculated from the magnitude-vs.-average displacement regression of Wells and Coppersmith (1994, all fault types), assuming that Mmax = 7.6 (+ 0.4, - 0.5). This yields mean values for average displacement of 1.3 m (0.2), 2.8 m (0.6), and 5.2 m (0.2). Mean recurrence is then calculated as mean displacement per event divided by mean slip rate. This procedure yields a mean recurrence of 75 kyr for the maximum earthquake, with

1-sigma limits of about +125 kyr and -50 kyr. The recurrence model we prefer is characteristic (weighted 100%).

3.3 BURIED STRIKE-SLIP FAULT SOURCE

Two lateral shear models were considered in our analysis of tectonic models, neither model is given much credibility based on data from the Yucca Mountain region. For the reasons discussed in Section 2, we give no weight to the transtensional nappe model. We apply a low, but non-zero, weight to the buried strike-slip fault (definition #2 in Section 2.1.5) as a seismic source. In general, the arguments in favor of a buried strike-slip fault include being in the region of the Walker Lane and invoking buried strike-slip faulting to explain the lateral component of slip on Yucca Mountain area faults. Arguments against such a fault include: lack of surface evidence for strike slip faults in the Yucca Mountain region, nor of any single, continuous strike-slip fault southeast of Crater Flat along the state line; vertical axis rotations in the area are variable in time and space and can be explained by normal faulting without any strike slip (C. Fridrich, SSC Workshop 3); and there is no evidence for large-scale offset (e.g., 25 km as suggested by Schweikert, at SSC Workshop 3) of volcanic rocks in Crater Flat.

Based on the above arguments, we consider it unlikely that a buried strike-slip fault exists. As shown in the logic tree in Figure ASM-1, whether such a fault exists is evaluated conditional on whether a detachment exists (as assessed previously). This is because, if a detachment exists, it would be more difficult to identify a strike-slip fault at depth. The detachment could serve to decouple the deeper lateral deformation from that occurring above the detachment. Assuming that a detachment does exist, the probability that a buried strike-slip fault exists is assessed to be 0.2; assuming that a detachment does not exist, the probability that a buried strike-slip fault exists is assessed to be only 0.05. This is because it is judged very unlikely that surface evidence for such a fault would have escaped detection during the field investigations in the region, especially assuming there is no detachment. Assuming that such a buried strike-slip fault exists, it could follow down-on-the-east segments along the west side of Crater Flat shown by John Bell (SSC Workshop 3) as part of a regional wrench system, or it could follow the location R. Schweikert designates—from Timber Mountain caldera to the south end of Crater Flat down the center of Crater Flat

(Schweikert, SSC Workshop 3). The hypothesized location of the buried strike-slip fault is shown on Figure ASM-3.

3.3.1 Seismogenic Potential

The next assessment is whether a buried strike-slip fault is seismogenic, given that it does exist. This assessment is judged to be conditional on the depth of the detachment lying structurally above the assumed strike-slip fault. (See discussion in Section 3.2.1 for the range of detachment depths as a function of the depth of the brittle crust). If the detachment is shallow, the probability that the strike-slip fault is seismogenic is relatively high (0.8); if the detachment is at moderate depth, the probability is 0.6; and if it is deep, the probability is 0. This assessment is based primarily on the observation that significant earthquakes on very long, thin (high aspect ratio) faults are not observed unless those faults penetrate the entire seismogenic crust.

3.3.2 Maximum Magnitude

Two estimates of rupture length are proposed to estimate maximum magnitude for a potential buried strike-slip fault. For the first approach, a 1932 Cedar Mountain earthquake-type rupture is assumed. The length of this rupture was about 60 km (Gianella and Callahan, 1934). Second, the length of Bell's down-to-the-east faults is assumed to represent a possible rupture segment for a strike-slip fault that is about 25 km long. Because the 25-km rupture length is based on local observations rather than a regional analogy, it is given higher weight (0.7) than the 60-km estimate (0.3). The magnitude associated with the 60-km rupture is 7.1 and with the 25-km rupture is 6.7, using the empirical relations between rupture length and magnitude of Wells and Coppersmith (1994).

Fault area also has an effect on maximum magnitude. Down-dip width of the buried strike-slip fault is conditional on the existence of the detachment. If the detachment exists, the range of possible widths of the buried strike-slip fault is based on combinations of estimated values of the detachment depth and thickness of the seismogenic crust. If no detachment exists, the upper limit of the buried strike-slip fault is assumed to be 7 km (just below the depth imaged on the seismic reflection profiles).

3.3.3 Recurrence

Earthquake recurrence is assessed based on the assumption that, if a buried strike-slip fault exists, its strain rate would be reflected at the surface by slip on the observed Yucca Mountain faults. Thus, we assumed the slip on this fault can be evaluated (or at least constrained) by using a geometrical relationship to the east-west extension associated with the Yucca Mountain faults. We resolve the total east-west extension (slip rates) for the faults of Yucca Mountain (i.e., Solitario Canyon, Windy Wash, Northern and Southern Crater Flat, Paintbrush Canyon/Stagecoach Road) onto a northwest-trending plane that has a pure lateral sense of motion. We assume three possible strike values for this plane (N20W, N35W, and N50W) with equal probability. A strike of approximately N35W appears to be the value indicated in Schweikert and Lahren (1997). There is uncertainty in this strike value. Hence we allowed a ± 15-degree variation in the strike of this source and assigned equal weights. This variation seemed permissible when compared to the somewhat general figures presented by Schweikert. The resulting values are:

Slip Rate = 0.1 mm/yr; Probability = 0.6
Slip Rate = 0.025 mm/yr; Probability = 0.2
Slip Rate = 0.24 mm/yr; Probability = 0.2

Given no constraints based on data for the behavior of this source, the characteristic recurrence model (Schwartz and Coppersmith, 1984; Youngs and Coppersmith, 1985) was assumed to be appropriate. This model has been shown to be appropriate for many individual faults.

3.4 LOCAL FAULT SOURCES

This section describes the local (i.e. within Crater Flat/Yucca Mountain/Bare Mountain area) fault sources considered in our preferred seismic source model (see discussion in Section 2.4). The description and characterization of the more regional faults (those outside the Crater Flat/Yucca Mountain/Bare Mountain area) is independent of the choice of local tectonic model. The more regional sources are described in Sections 3.5 and 3.6. The faults included in our evaluation (regional and local) are a subset of those identified in Piety (1995) and H. L. McKague *et al.* (CNWRA, written communication, 1996). Some faults in those compilations were omitted from consideration based on a lack of Quaternary activity in Chapter 11 of the

summary report (USGS, written communication, 1996), or those more regional faults that Anderson *et al.* (1995a,b) considered to lack evidence for Quaternary activity.

The regional and local faults are evaluated according to the probability that they are seismogenic. Given that they have some probability of being seismogenic, their location and extent are evaluated, behavioral aspects assessed, maximum magnitudes defined and recurrence evaluated.

3.4.1 Seismogenic Potential

The evaluation of which mapped faults to include as seismic sources is a function of the interpretation of the seismogenic potential (probability of activity) of each fault. The criteria we used to evaluate whether a fault is seismogenic are: (1) the recency of slip on the fault; this is the strongest criterion but is difficult to determine in this area because of long recurrence intervals; and (2) the length of the fault, which should be long enough to generate magnitude 5 to 52 earthquakes (approximate length of 5 km); and (3) the interpreted average late Quaternary displacement. Other observations that are potentially important include evidence of brittle slip in the geologic past and involvement in development of throughgoing structures. If a fault was active in the geologic past but is truncated downdip, we consider it will not become active as an independent source again.

Northwest-Trending Faults. The mapped northwest-trending faults in the site area (i.e., Drillhole Wash fault, Sever Wash fault, Pagany Wash fault, and Yucca Wash fault) are assessed to be nonseismogenic based on their short lengths (3 to 5 km), no evidence for Quaternary displacement, and a slip tendency that is not favorable within the present stress regime (Stamatokos and Ferrill, SSC Workshops 3 and 4; H. L. McKague *et al.*, CNWRA, written communication, 1996). We consider the regional seismic source zone to incorporate the hazard from small faults of these dimensions.

Ghost Dance Fault. The Ghost Dance fault is oriented favorably for slip but there is no evidence that it is active or seismogenic. Within a resolution of less than 0.5 m, slip in the past approximately 300 ka is precluded by the lack of displacement of a bedrock paleosurface (E. M. Taylor *et al.*, written communication, 1996a). During the same time, multiple paleoearthquakes are recorded along the nearby Solitario Canyon fault. The northern

terminus of the fault is identified from detailed mapping, and it appears to be truncated by a structure to the south. Therefore, the length of the fault is comparable to that of the northwest-trending faults. Further, its geologic history does not suggest that it was a zone of significant localized slip. On the basis of these arguments, the Ghost Dance fault is assessed to have a probability of zero that it is seismogenic.

Sundance Fault. The 700-m-long Sundance fault is too short to be an independent seismic source. There is also no evidence for Quaternary slip.

North-Trending Faults. We have identified nine local faults as seismic sources near Yucca Mountain (Figure ASM-4). Four of these faults (Bare Mountain, Windy Wash, Solitario Canyon, and Paintbrush Canyon/Stagecoach Road) are termed major, block-bounding faults and are interpreted to penetrate the entire seismogenic crust. {Note: we characterize the Paintbrush Canyon/Stagecoach Road faults as a single fault.} The remaining north trending faults (Northern and Southern Crater Flat, Fatigue Wash, Iron Ridge, Bow Ridge) are termed minor or secondary faults; they likely merge with the major, block-bounding faults within the seismogenic crust. Our characterization of the local Crater Flat Group (CFG) faults is summarized on Figure ASM-5. We interpreted all the major, block-bounding faults listed above to be seismogenic (probability = 1.0). The probabilities that minor faults are seismogenic are based on the sizes of per-event displacements inferred from trenches (see Section 3.4.3.1 and Table ASM-1). The mean and maximum of $D_{preferred}$ values and the probability that the fault is NOT seismogenic are as follows: Bow Ridge fault (24, 44 cm, and 0.3); Northern Crater Flat fault (47, 50 cm, and 0.2); Southern Crater Flat fault (20, 20 cm, and 0.5); Fatigue Wash fault (61, 105 cm, and 0.1); and Iron Ridge fault (80, 100 cm, and 0.1).

3.4.2 Geometry Models

Fault Rupture Lengths. For the nine local faults that we characterized in detail, we made three estimates of maximum surface rupture length to evaluate the maximum earthquakes (Table ASM-2). The minimum length equals the along-strike distance between the farthest-apart points on the fault that display Quaternary displacement indicated on the map of Simonds *et al.* (1995). The preferred length is the along-strike distance between the ends of the obvious mapped fault (irrespective of age of displacement) as shown on the fault map

of Simonds *et al.* (1995). The maximum length is the along strike distance between the maximum inferred limits of mapped bedrock fault(s), as shown on the Simonds *et al.* (1995) map. On the north, most of the faults are interpreted to be truncated by the northwest-trending faults (Yucca Wash, etc.).

Because we want the length of surface rupture during the maximum earthquake, we considered it unlikely that such a rupture would be limited to a minimum length defined by distance between trenches as postulated in Table 5.1 of the synthesis report (USGS, written communication, 1996), for two reasons: (1) the distance between trenches showing Quaternary offset is a minimum estimate for the length of Quaternary faulting, and the maximum earthquake should have a maximum (rather than a minimum) rupture length; and (2) depending on how the trenches were sited (e.g., some are clustered near roads), their spacing may show only a small extent of the Quaternary surface rupture. We give this interpretation a zero weight. We consider that the maximum earthquake would cause rupture at least equivalent to the extent of faulted Quaternary deposits. The longest possible surface rupture length in the maximum earthquake is constrained by the mapped length of the fault in bedrock. We estimate a 30 percent probability that the maximum earthquake could rupture the entire mapped extent of the fault and at least some distance beyond on along-strike structures inferred as faults on the Simonds *et al.* (1995) map.

Downdip Extent of Faults. To compute downdip width (and hence fault area), dips on the major, block-bounding local faults were interpreted to range from 45 to 70 degrees. These values are based on observed surface dips in the Basin and Range, theoretical considerations for normal faulting (Sibson, 1985), surface dips in the Yucca Mountain area (C. Fridrich, SSC Workshop 2), the seismic reflection profiles (presented by T. Brocher, SSC Workshop 2), and the observations of seismicity from the Little Skull Mountain sequence (K. Smith, SSC Workshop 2).

As described above, our assessment divides the local faults into two categories: major, block-bounding faults (which include the Bare Mountain, Solitario Canyon, Paintbrush Canyon/Stagecoach Road, and Windy Wash faults), and secondary faults (which include the Northern and Southern Crater Flat, Fatigue Wash, Iron Ridge, and Bow Ridge faults). The block-bounding faults are of sufficient length that they may fully penetrate the seismogenic

crust. This interpretation is based on the overall length of the block-bounding faults, reasonable aspect ratios given those lengths, and total displacement across the faults. Hence the area for these faults is conditional on the seismogenic crustal thickness or existence of a detachment, fault dip, and maximum rupture length. For the secondary faults, downdip width was assessed assuming an aspect ratio (AR) for the fault (horizontal/vertical) in the range of 0.91 to 2.2 based on data presented in Nicol *et al.* (1996). Dip values for the secondary local faults were assumed to be in the range of 65 to 75 degrees. These values for dip of the secondary faults are based simply on the observation from structural cross sections and seismic reflection data from normal faulting terranes that secondary faults that merge with more significant faults (in terms of structural offset) commonly have steeper dips than the associated major fault. Hence we characterize a slightly steeper dip for the secondary faults.

Our evaluation of the downdip geometry considers two basic alternatives, one with many of the faults merging at depths above the brittle-ductile transition and one with individual, planar faults that do not intersect (Figure ASM-5). Based upon the spatial proximity and anastamosing pattern of the local faults in map view, we assign a high probability (0.95) that the faults merge within the seismogeneic crust. Conditional on the existence of a detachment we assign 1.0 probability that the faults merge down dip. Note that for the interpretation that a detachment exists, then all of the local faults are limited in their depth extent by the detachment depth.

A number of geometries are considered possible for the merging case, the major, block-bounding faults (Bare Mountain, Paintbrush Canyon/Stagecoach Road, Solitario Canyon, and Windy Wash) are evaluated for likelihood of interrelationships with the secondary faults and with each other based on aspect ratio and geometry (as discussed by C. Fridrich in SSC Workshops 2 and 6). As indicated on Figure ASM-6, a large number of possible geometries were considered based on ranges of dip and aspect ratio for the secondary faults and dips for the primary faults. Cross-sections for both northern and southern transects were constructed with weights for aspect ratios and dips as described above.

The result was the development of four representative cross-sections that define the uncertainty in downdip geometry of the block bounding and secondary faults (Figures ASM-5 and ASM-7). If the faults merge down dip, then three alternative geometries are defined: a

shallow model, a preferred model, and a deep model. These models reflect the depth at which merging takes place. The dip of the faults is assumed to increase as the depth of merging increases (see Figure ASM-7). Based on the weights assigned to fault dips and aspect ratios, the weights assigned to the shallow, preferred and deep merging models are 0.1, 0.6, and 0.3 respectively. For the nonmerging case, only one model is considered because steep fault dips are required to maintain fault separation throughout the seismogenic crust. In the nonmerging case, the downdip extent of the secondary faults is limited by the preferred AR value of 1.55 (the central value of the range quoted earlier).

3.4.3 Behavioral Models

Our evaluation of the behavioral aspects of the Yucca Mountain faults focused on displacement and temporal attributes.

Maximum and Average Displacements in the Maximum Earthquake. Several procedures were utilized to estimate average and maximum displacements for each local fault source from the Yucca Mountain trench data. (Note: All data to develop these parameters is from Table 5.1 of the synthesis report (USGS, written communication, 1996). By using the several methods we intend to capture the uncertainty in models (methods) as well as sampling and interpretation uncertainties.

Average Displacement- One method to estimate the average displacement, D_{avg}, is simply to average the preferred values of displacement, D_{pref}, from all events in all trenches along each fault. An alternative is to average the D_{pref} values from the largest event on each fault. We have computed true D_{avg} using each of these techniques and assigned a weight of 0.5 to each result. The results are contained in Table ASM-1.

Maximum Displacement- One technique is to simply take the largest value of D_{pref} in any trench on the fault to represent the maximum displacement in the earthquake, true D_{max} (we distinguish true D_{max} from the maximum estimates of displacement for each event in each trench). However, based on the Borah Peak results, only 2-3% of the fault trace exhibits displacements within 80-90% of the true maximum displacement value. Hence, it is unlikely that even three randomly placed trenches would sample within 80-90% of the true maximum

displacement. We give this technique for estimating true D_{max} a weight of 0.25. An alternative method to estimate true D_{max} is to consider choose the largest displacement value from Table 5.1 for each fault. This incorporates the uncertainty in interpretation/evaluation of displacements within the trenches. We have assigned a weight of 0.5 to this technique. Another way to estimate true D_{max} is to consider it a multiple of true D_{avg}. This is a technique suggested by Mason (1996). At Borah Peak, the ratio of true D_{max}/D_{avg} is ~3.37 for the entire 33.8 km of the surface rupture, for the central portion of the fault it is ~2.59. Our alternative technique is then to take each of the true D_{avg} values described above and multiply them by 2.59 to arrive at values for D_{max}. We have assigned a subjective weight of 0.125 to each of the resulting values. Using this procedure we attempt to reduce the uncertainty due to sampling bias (i.e. trench location). The results for true D_{max} also are contained in Table ASM-1.

Simultaneous Rupture of Fault Sources. For this analysis, "simultaneous rupture" is defined as ruptures on two or more faults occurring within 30 seconds of each other. Hence, simultaneous rupture increases the magnitude of the earthquake. In effect, the *areas* of the faults involved are combined to contribute to a larger magnitude. We take this rather strict definition because the purpose of this characterization is to evaluate vibratory ground motion hazard. If two or more faults rupture more than ~30 seconds apart (i.e. strong motion from the second fault begins arriving at the site after shaking from the first event has stopped) the two earthquakes (occurrence) can be characterized as independent events. The logic tree that defines the structure and uncertainties in this assessment is given on Figure ASM-5 and is described below.

The potential for simultaneous rupture is dependent upon whether or not the faults merge down dip. If the faults do not merge, then it is assumed that simultaneous ruptures do not occur (Figure ASM-5). In addition, the probability that simultaneous ruptures occur is assessed based on the likelihood of temporal overlap during past events. Based on the results presented in the synthesis report (as presented by Pezzopane and Whitney, SSC Workshop 3) and as summarized by L. Anderson (in SSC Workshop 4) the potential simultaneous ruptures considered are listed on Figure ASM-8. We assigned probabilities to the scenarios listed in Table 5-3 of the synthesis report as follows: high confidence cited in Table 5-3 received a

P=0.9, moderate confidence received a weight of 0.5, and low-moderate confidence received a weight of 0.25. Then for each fault pair, these values were multiplied times the fractional number of total events on the two faults that were inferred to be in common to compute a probability of temporal overlap for the fault pair. The ultimate probability of simultaneous rupture (under our definition) is then the linked probability of the geometry and temporal overlap branches. This result is a probability of 0.3 that simultaneous ruptures occur, given that the faults merge down dip (Figure ASM-5).

3.4.4 Maximum Magnitude

Maximum earthquake magnitudes for the independent fault sources were assessed using maximum rupture dimensions (surface rupture length, displacement, area) for individual maximum events, as discussed above. Our parameters included surface rupture length, maximum and average displacement per event, rupture area, and displacement times length vs. magnitude (Mason (1996); see Table ASM-3). For the local faults, the subjective weights for each of the above methods used to compute magnitude estimates was applied individually, i.e., was given a fault-specific set of weights. We gave the highest weights to the surface rupture length (SRL) relationship of Wells and Coppersmith (1994) and SRLxD method of Mason (1996), each assigned a weight of 0.3. Weights of 0.15 were applied to the average and maximum displacement methods, and a weight of 0.1 was applied to the rupture area method (all from Wells and Coppersmith, 1994).

These general rules were modified on a fault-specific basis (Table ASM-3) for several reasons. First, on some faults no average displacement values could be calculated, because there was only one trench for which displacements were reported. In such a case, we could not estimate magnitude based on average displacement. Second, if the displacements in individual trenches ranged greatly from event to event, we had a low confidence that a computed average displacement was meaningful. Given the large variability of displacement along strike in historical normal surface ruptures (e.g., Wheeler, 1989; McCalpin, 1996), we generally had low confidence that a few randomly sited trenches would fortuitously sample either the maximum or average displacement for each paleoearthquake. Thus, magnitude estimates based on displacements usually were assigned lower weights than estimates derived by other methods. Third, if faults were so proximal at the surface that they could merge downdip within the crust, we acknowledged greater uncertainty in their downdip extent, and

thus lowered the weight on estimates based on rupture area. Finally, for faults that possess short lengths with respect to their observed per-event displacements, we generally assumed that: (1) the faults must fully penetrate the crust to explain such large coseismic displacements; (2) if the faults fully penetrate the crust, they must have a downdip dimension of 14 to 20 km (assuming a 60-degree dip and 12 to 17 km depth); (3) it would be very unusual for a fault having a 14- to 20-km downdip extent to be shorter than 14 km, because that would imply an aspect ratio of less than 1.0; therefore, (4) those faults were considered to have longer ruptures than the mapped fault length, by linking with other mapped faults; and thus (5) the large displacements considered were more representative of the maximum earthquake than the short lengths of the mapped faults. [We note that the definition and naming of separate faults in an anastomozing network of faults, such as exists at Yucca Mountain, is somewhat arbitrary. This is the reason we have chosen to consider the Stagecoach Road/Paintbrush Canyon system as a single fault. Based on the large reported displacements, short length and along strike geometry of the Stagecoach Road fault we infer it to be connected at depth with the Paintbrush Canyon fault].

For each fault, we evaluated the quality of the data on fault dimensions and then altered the weighting outlined above to reflect our assessment of believability in the measurements.

3.4.5 Recurrence

Fault Slip Rates. Slip rates were assessed using data in Table 5.1 of USGS (written communication, 1996). First, the long-term mean slip rate for each fault was computed (including data uncertainties), and a normalized-grouped cumulative density function (CDF) was generated, after the technique of McCalpin (1995). Examples of this technique are provided in Appendices ASM-1 and ASM-2. This technique considers the variation of slip rates among many faults over a short period to mimic the variation on a single fault over a longer period. The mean long-term slip rate is applied to the CDF to produce a fault-specific CDF of slip rate. Values of the 20-percentile, median, and 80-percentile are listed in Table ASM-4. The full CDF was used in the analysis.

Earthquake Recurrence. Two alternative approaches were used to characterize earthquake recurrence relationships for independent fault sources. In the first approach, the inter-event times from Table 5.1 of the USGS (written communication, 1996) are used, along with the

errors cited for the "preferred, maximum, and minimum" estimates, to calculate the times between characteristic paleoearthquakes. The cited values are considered to represent only measurement error for a given interval, and not the stochastic variability between successive events in a given trench.

To account for the stochastic variability, we again used the McCalpin (1995) approach. Normalizing all recurrence data by setting the long-term mean recurrence of each fault to 100 ka. We then grouped all normalized recurrence intervals for all faults and plotted the cumulative density function (CDF). Probability density functions and cumulative distributions for this technique are contained in Appendices ASM-3 and ASM-4, respectively. (This same approach was used for slip rate; see McCalpin [1995] for explanation of the technique.) We then input the long-term interevent time for each fault (which contains only measurement errors) into the CDF to produce a new CDF that incorporates both measurement error and stochastic variability, as contained within the normalized-grouped data set (Appendix ASM-5). These values are listed in Table ASM-5. This approach is given a weight of 0.5, which reflects our evaluation that it is an equally valid approach to the slip rate approach described below. This approach yields only the recurrence times between maximum (or characteristic) earthquakes; frequency of smaller earthquakes is derived from the recurrence models described below.

In the second approach, the slip rate distributions described above are used to develop recurrence relationships using a moment rate approach (e.g. Youngs and Coppersmith, 1985). This approach was also given a weight of 0.5.

The application of the slip rates and recurrence intervals to develop recurrence rates for the local faults depended upon the behavior model. Under the condition that simultaneous ruptures do not occur, the individual faults are assumed to act independently, and the assessed slip rates and recurrence intervals for each fault are used to define the recurrence relationship for the fault. Under the condition that simultaneous ruptures can occur, then the slip rates and recurrence intervals are partitioned between individual fault ruptures and simultaneous fault ruptures as follows.

Listed on Figure ASM-8 are the assessed percentage of fault ruptures on the individual block-bounding faults that are considered to be simultaneous ruptures with other faults and the relative frequency of various fault rupture combinations. The slip rate that is released in multiple-fault rupture is set equal to the assessed fault slip rate times the percentage of times the fault ruptures simultaneously with other faults. This slip rate is further partitioned among the various multiple-fault rupture scenarios by the relative frequencies listed on Figure ASM-8. For example, under the condition that simultaneous ruptures occur, 90% of major ruptures on the Bare Mountain fault are assumed to be simultaneous ruptures and 1/3 of these are in combination with the Solitario Canyon fault. Similarly, 70% of ruptures on the Solitario Canyon fault are assumed to be simultaneous ruptures and 1/2 of these are in combination with the Bare Mountain fault. The assessed slip rate used to define the recurrence of simultaneous ruptures of the Bare Mountain and Solitario Canyon faults is set equal to 30% of the Bare Mountain slip rate plus 35% of the Solitario Canyon slip rate.

The assessed recurrence rates for individual faults are similarly partitioned; 30% of the rate for Bare Mountain events are assumed to be simultaneous ruptures with Solitario Canyon and 35% of the rate for Solitario Canyon events are assumed to be simultaneous ruptures with Bare Mountain. Because these assessments are approximate, the computed frequencies were not identical, and an average of the two values was used to define the recurrence rate for the simultaneous ruptures.

Under the condition that simultaneous ruptures can occur, the slip rates and recurrence intervals for individual fault ruptures are set equal to the assessed values for the individual faults times the percentage of times that individual fault ruptures occur (e.g. for Bare Mountain 10% of the ruptures are assessed to be independent ruptures of the Bare Mountain fault).

For the local faults, three recurrence models were used. The highest weight was given to the characteristic model of Schwartz and Coppersmith (1984) (as described by Youngs and Coppersmith, 1985), weight = 0.7; the exponential recurrence model was assigned a weight of 0.2; and the "maximum magnitude" model (similar to Wesnousky *et al.*, 1983) was assigned a weight of 0.1

In constructing the recurrence relationships we assume that the maximum magnitude assessments described in Section 3.4.4 are the central value for the characteristic magnitude interval (e.g. Youngs *et al.*, 1987). For the characteristic and maximum moment recurrence models, the characteristic events are uniformly distributed in the magnitude range M_{max}±¼, such that the upper limit of the recurrence relationship is M_{max}+¼. For the exponential recurrence model the upper limit is also set at M_{max}+¼. When the recurrence relationship is specified by the recurrence interval of surface-rupturing earthquakes, this recurrence rate was assumed to apply to earthquakes of magnitude greater than or equal to M_{max}-¼.

Under the condition that simultaneous ruptures can occur, the above three recurrence models were used to assess the relative frequency of various magnitude earthquakes for individual fault ruptures only. Multiple fault ruptures were assumed to be additional, larger events and the assessed maximum magnitude earthquakes were assumed to be the only events occurring.

3.5 REGIONAL FAULT SOURCES

Regional fault sources include regional faults (i.e., those outside the immediate Yucca Mountain/Bare Mountain/Crater Flat area) within 15 to 100 km from the site that are judged to be relevant earthquake sources. The locations of these regional fault sources are shown on Figure ASM-9. Most of the faults are listed in Table 11-1 in chapter 11 of USGS (written communication, 1996). We include, in addition:

(1) Carrara (or U. S. Highway 95) fault,
(2) East Specter Range fault,
(3) a 12 km northern extension of the West Spring Mountains fault,
(4) Middle Death Valley fault, and
(5) West Death Valley fault.

Regional geologic, seismologic, and geophysical studies, and evaluation of these faults suggest that they are steeply- to moderately-dipping faults and exhibit conjugate relationships as discussed in Section 2.2. The northwest-trending faults are generally right-lateral and lie within the Walker Lane (Stewart, 1987) west of Yucca Mountain. Regional fault sources in the Basin and Range province east of the Death Valley-Furnace Creek-Fish Lake Valley fault zone have slip rates that are about one or more orders of magnitude lower than the faults within the Walker Lane.

Several other regional faults were excluded from our analysis based on: (1) data presented by Anderson *et al.* (1995a) that showed little evidence for middle to late Quaternary activity (e.g., Keane Wonder, Oasis Valley, Rocket Wash/Beatty Wash, and the Toliche Peak faults); or (2) sparse documentation of Quaternary activity (e.g., the Tin Mountain, Tikaboo, Stonewall Mountain, and Racetrack faults). The Kawich Range fault was excluded based on the discussion in Anderson *et al.* (1995a) and consideration of the short length of known Quaternary faulting. An estimated Mw 6.82 earthquake (based on SO = 1.5 m displacement at profile KRW-3) on this fault at about 72 km from the site would not be a relevant event on Figure 11-3 of Pezzopane (in USGS, written communication, 1996).

Table ASM-6 summarizes the earthquake source characteristics for the 24 active regional faults that are included in our source model. This table is revised from the table in the memorandum from the ASM team of 13 May 1997, titled A Revised Source Data for Regional Faults (ASM Team). With the exception of the Carrara fault, all sources are assigned a probability of 1.0 of being seismogenic based mainly from paleoseismic evidence summarized in Anderson *et al.* (1995a, b), R. E. Klinger and L. A. Piety (USBR, written communication, 1996), Piety (1995), and various chapters of USGS (written communication, 1996). The Carrara fault is judged to be seismogenic with a high probability (0.85) for the reasons cited in Appendix ASM-6, but because the fault has not been fully characterized, some probability (0.15) is given to the possibility that it is not seismogenic. A generalized planar fault geometry to seismogenic depth was assumed for all the regional fault sources. Predominantly strike-slip faults are modeled as having a dip of 90 degrees. Predominantly normal or dip-slip faults are modeled as having dips of 60 degrees.

3.5.1 Estimation of Quaternary Ages

The ages of fault activity of Table 2 in Anderson *et al.* (1995a, b) were used as a starting point. Our evaluation considered that: (1) the Pleistocene/Holocene boundary may be nearer 12 than 10 ka; (2) many references use 125 or 130 ka for the boundary between late and middle Pleistocene (128-770 ka); (3) the boundary between middle and early Pleistocene is 770 ka, and early Pleistocene is 770 to 1650 ka, which strongly skews the middle Pleistocene toward the present, and the middle Pleistocene is already skewed toward the present based on a start at 1650 ka bp, or more than 2000 to 2400 ka based on some recent dating. The

terminology may be misleading as the middle Pleistocene includes the most recent 8-47 percent of the Pleistocene (using 1650 ka), and does not include even the middle of the Pleistocene. It is however, the most widely used classification, and is required for comparative purposes. Accordingly, the following approximate dates are used in our analysis:

(1)	Holocene/late Pleistocene boundary =	10 ka
(2)	latest Pleistocene (avg. of 10 ka and 28 ka) =	19 ka
(3)	latest Pleistocene (avg. of 10 ka and 69 ka) =	39 ka
(4)	mid-late Pleistocene (avg. of 10 ka and 128 ka) =	69 ka
(5)	late Pleistocene/middle Pleistocene boundary =	128 ka
(6)	middle Pleistocene = (avg. of 128 and 770 ka) =	449 ka
(7)	middle Pleistocene/early Pleistocene boundary =	770 ka
(8)	beginning of Pleistocene =	1650 ka

3.5.2 Maximum Magnitude

Maximum magnitudes were calculated using an empirical relation that relates surface rupture length (SRL) to magnitude (Wells and Coppersmith, 1994, for all fault types). The relationship for all fault types was used because the data base is more robust, has a lower standard deviation, and higher correlation coefficient than for normal faults, and the relationship for strike slip, normal slip, and all fault types are almost coincident as shown on Figure 9 (b), and Table 2A of Wells and Coppersmith (1994). The uncertainty in maximum magnitudes is represented by the range of minimum, preferred, and maximum SRL. This uncertainty is approximately +/- 0.2-0.4 magnitude unit for 9 of 26 faults, and is lower for the other faults where SRL is constrained by intersection or connecting faults, or consistent magnitude values are obtained from maximum displacement or average displacement values.

3.5.3 Slip Rate

Two approaches were used to estimate slip rates for regional faults. For well- to moderately well-studied faults (designated by italic font in Table ASM-6) reported slip rates were used, with most preferred values assigned a weighting of 0.6 to 0.8, and maximum or minimum values of 0.1 to 0.2. For faults that have poor or incomplete characterization data (designated by normal font in Table ASM-6), slip rate was estimated from surface rupture length as described below. The weightings for these values have greater uncertainty than for the relatively well-studied cases. We thus assigned equal weight (approximately 0.33) to the preferred, maximum, and minimum values.

Slip Rate Estimated From Surface Rupture Length. The average slip rate for the faults that have relatively good SRL or length estimates and the approximate age of disturbed geomorphic surfaces as summarized in Piety (1995) were made as follows:

1. Maximum displacement (MD) for each event is estimated from surface rupture length (SRL) using the following relationship from Wells and Coppersmith (1994): log (MD) =-1.38 + 1.02 log (SRL). This relationship is based on a robust worldwide database of 95 events, and has a good coefficient of correlation of 0.75 and a standard deviation of 0.41. The regressions in Wells and Coppersmith (1994) generally are based on the maximum observed horizontal, oblique, and/or vertical surface displacement.

2. MD is multiplied by 0.38 to obtain AD, the average displacement (in mm). The multiplier value used is based on the average of values presented in Mason (1996) for Basin and Range normal faulting events, Slemmons (unpublished data for all fault types, and Basin and Range events), and Strom and Nikonov (unpublished data for normal faulting events) as summarized in Table ASM-7.

3. An assumed number of surface rupture events is inferred. Based on field data and observations for better studied regional faults (Table ASM-8) a value of 3 events is used in the analysis for the average number of surface faulting events.

4. Cumulative displacement is estimated by multiplying the estimated AD by 3 (the inferred number of surface rupture events).

5. An estimated slip rate is calculated using the cumulative displacement divided by the estimated ages for the geomorphic surfaces that are displaced by the fault. The displaced surfaces generally are assumed to be late to middle Pleistocene and equal weight is assigned three ages (69 ka, 128 ka, and 449 ka) (see Section 3.5.1 for discussion of estimated ages). The interval of time used is truncated at 10 ka, since mid-Holocene events appear to be absent from the faults, but early Holocene, or late Pleistocene events are present on some of the faults. Therefore, values of 59, 118, and 449 years were used to calculate maximum, preferred, and minimum slip rates.

3.5.4 Recurrence Intervals

C. M. dePolo and D. B. Slemmons (Nevada Bureau of Mines and Geology, written communication, 1997) previously examined the ten largest surface rupture areas in the Basin and Range province for earthquakes of Mw = 6.3 to 7.5, including (Owens Valley; Sonora, Mexico; Pleasant Valley; Hansel Valley; Cedar Mountain; Rainbow Mountain; Fairview

Peak; Dixie Valley; and Borah Peak earthquakes. All areas showed prominent Holocene and late Pleistocene paleoseismologic features along most scarps. Approximately 90 percent of the historical surface faults coincided with paleoscarps. This recurrent activity also is reported for most of the Yucca Mountain Quaternary faults, with all of the larger fault scarps showing geomorphic evidence for multiple events on at least parts of the fault zone. This multi-event relationship is better expressed in the exploratory trenches, and for the higher slip rate, most recently active faults, than by faults that have low slip rates and extremely long recurrence intervals (e.g., > ~ 100 kyr). Based on these observations, we assumed multiple events in our assessment of recurrence intervals for regional fault sources.

Two approaches were used to estimate recurrence intervals for regional faults: (1) for well-studied faults (designated by italic font in Table ASM-6) estimates of recurrence interval were obtained from paleoseismic data reported in the references provided and from personal observations by D. B. Slemmons as discussed in Appendix ASM-6; and (2) for faults with little or no paleoseismic data (designated by normal font) the recurrence intervals were estimated as follows.

The scarps observed in middle to late Pleistocene surfaces (based on data in Piety, 1995 and observations of D. B. Slemmons as discussed in Appendix ASM-6) are assumed to result from multiple surface faulting earthquakes. An assumed number of surface rupture events is inferred. Based on field data and observations for better studied regional faults (Table ASM-8) a value of 3 is used in the analysis for the average number of surface faulting events.

Three values (69 ka, 128 ka, and 449 ka) are used for the estimated age of the displaced geomorphic surfaces. As noted in the previous section, 10 kyr have been subtracted from these ages to estimate the pre-Holocene duration of time during which the inferred three events occurred.

The estimated duration periods of 59, 118, and 439 years are divided by 3 (the assumed number of surface rupture events) to provide the following estimated values and weights for recurrence interval: 20 kyr (0.33), 39 kyr (0.34), and 146 kyr (0.33).

In some cases (e.g., the Emigrant/Towne Pass and Grapevine faults) additional data that are available to constrain the timing of the most recent event, or possibility of connecting with

other fault extensions, also were incorporated into the assessment of recurrence interval as described in Appendix ASM-6.

3.5.5 Recurrence Models

Two recurrence relations were used to characterize the regional fault sources: the maximum moment recurrence model (Wesnousky, 1986) and the characteristic earthquake recurrence model (Youngs and Coppersmith, 1985). The maximum moment recurrence model was derived by Wesnousky (1986) from paleoseismic data for faults in southern California region, and this method, which was deemed most appropriate for our regional fault evaluations, was given a weighting of 0.8. The Youngs and Coppersmith model is widely used, but is more appropriate for earthquake catalog data. Since it is a widely used method, we felt it should be considered but assigned it a lower weighting of 0.2. The recurrence models are applied in the same manner as was done for the local sources.

The characteristic model requires estimates of the b-value associated with specific faults. The b-values used varied from fault to fault depending on the values assigned to the areal source zone in which the individual fault lies (see below).

3.6 REGIONAL SOURCE ZONES

Six regional source zones were defined within 300 km of the Yucca Mountain site for this evaluation: a Basin and Range zone, a Walker Lane zone (which contains the Yucca Mountain site), a Colorado Plateau zone, a Mojave block zone, a San Andreas zone, and a Sierra Nevada/Basin and Range zone (see Figure ASM-10). These zones are based on tectonic characteristics, style of faulting, and observed seismicity rates. From west to east the 300 km radius of the Yucca Mountain site) is divided into the following source zones:

Sierra Nevada/Basin and Range Boundary Zone. This en echelon zone includes the Mw=7.5 Owens Valley earthquake of 1872 (Beanland and Clark, 1994), that accommodates a significant fraction of the inferred activity of the Eastern California Shear Zone (Savage *et al.*, 1990) and high seismic activity rate of the southern portion of the Central Nevada Seismic Zone (Rogers *et al.*, 1991).

Walker Lane. This zone, defined by (Stewart, 1987), includes the Basin and Range Province of highest activity from Owens Valley to Death Valley, and a narrow eastern Walker Lane of lower tectonic and seismic activity from Death Valley to Yucca Mountain.

Yucca Mountain Subzone. A subzone of 50 km radius within the Walker Lane surrounding the Yucca Mountain site. Defined on the basis of enhanced geological investigations.

Basin and Range Province. The Basin and Range Province northeast of Walker Lane, which at the Yucca Mountain latitude has a much lower rate of activity than the Walker Lane. Dominated by north-trending normal faults and moderate to high seismic activity rate.

Colorado Plateau. The relatively stable block along the southeast boundary of the Basin and Range Province, more than 200 km east-southeast of Yucca Mountain.

Mojave Block. A relatively stable block generally south of the Garlock fault (about 100 km south of Yucca Mountain), which forms a boundary between the Walker Lane and Sierra Nevada/Basin and Range Province, and the Colorado Plateau Zone.

San Andreas Fault System. The highly active right-lateral fault system, which accommodates about 75 percent of the differential movement between the North American and North Pacific plates.

For characterization of seismic sources we used those source zones that extend within 100 km of the site as shown on Figure ASM-11 (these are the Walker Lane and Basin and Range Province).

3.6.1 Recurrence

For each zone, the recurrence is assessed to follow a truncated exponential form with probability of one. Although individual faults may follow a characteristic or maximum moment recurrence relationship, regions (i.e., source zones) generally are well represented by the truncated exponential model of earthquake recurrence (Youngs and Coppersmith, 1985; Richter, 1958).

The recurrence for each zone is computed using the appropriate subset of the 300-km catalog, declustered using the Veniziano and van Dyke (1985) (as described in McGuire, 1985) (weight =0.7) and Youngs *et al.* (1987) (weight=0.3) techniques (see Appendix D of the main report). The catalog declustered using the Veniziano and van Dyke approach is referred to as Version 7, the catalog declustered using the Youngs *et al.* approach is referred to as Version 5. Based on comparisons of the space-time plots, the Veniziano and Van Dyke (1985) technique appears to be more successful at declustering the catalog and has been weighted higher. Additional attempts at declustering were made using the technique of Reasenberg (1985). This technique was significantly less successful at declustering the catalog (see example space-time diagrams in Figure ASM-12). As a result, the Reasenberg algorithm was not utilized to develop recurrence statistics for the source zones. Data after 1950 from the region within the Nuclear Test Site (Figure ASM-11) where nuclear testing was performed was removed from the recurrence computations to remove the influence of induced events. Completeness intervals were estimated using existing literature (Gomberg, 1991b), comparisons of "Stepp-plots" (Stepp, 1972) (example shown in Figure ASM-13) from the catalog along with consideration of the operational history and sensitivity of instrumentation in the area (personal communication, 1997; A. Rogers, J. Brune, K. Smith). The assessed completeness intervals for the 100 km radius around Yucca Mountain are summarized below.

M 2.0-2.5	1983-present
M 2.5-3.0	1979-present
M 3.0-3.5	1961-present
M 3.5-5.0	1932-present
M 5.0-6.0	1900-present
M 6.0-6.5	1880-present

3.6.2 Maximum Magnitude

Within the broader Walker Lane zone, a subzone (the Yucca Mountain subzone) is defined by a 50-km radius around the Yucca Mountain site. Given the extensive investigations in this area, it seems unlikely that any significant (in terms of slip rate), young, potentially surface rupturing faults have escaped detection within this zone. Hence we assign a lower maximum magnitude to this part of the Walker Lane zone. We assign a maximum magnitude of 6.3 +/- 0.3 to this source. We consider this value to represent the approximate upper limit magnitude for non-surfacing rupturing earthquakes in this sub-zone. Based upon the work of C.M. dePolo, University of Nevada, Reno (written communication, 1996, and as presented in SSC

Workshop 4) and considerations of physically reasonable fault area/displacement/stress drop considerations (as presented by J. Ake at SSC Workshop 4). The logic tree used to characterize the regional source zones that lie within a 100-km radius of the site is shown on Figure ASM-14.

Estimates of maximum magnitudes for source zones (other than the Yucca Mountain source subzone) were assigned based either on the inferred surface rupture length of the largest fault not explicitly characterized with the regional faults or the maximum magnitude event inferred to have occurred historically in that zone. It is our assessment that some potentially seismogenic faults are not represented in the list of regional faults specifically included in the source model (Table ASM-6 and discussed in Section 3.5). Some of these faults lack recurrence information. We used the maximum magnitude suggested by either: the approximate maximum length of those faults or the largest earthquake in the zone, to constrain the maximum magnitude for the zone in question. The maximum magnitudes for each of the seven source zones are summarized below:

Basin and Range	Mmax = 7.2
Walker Lane	Mmax = 6.8
Yucca Mountain subzone	Mmax = 6.3
Colorado Plateau	Mmax = 7
Mojave Block	Mmax = 7.7
San Andreas	Mmax = 8
Sierra Nevada/Basin and Range	Mmax = 7.6

Uncertainty in the maximum magnitude was assumed to be ±0.3 units at the 90 percent confidence interval.

3.6.3 Stationarity of Seismicity

When characterizing the seismic hazard within a source zone, two alternative hypotheses are commonly used. One considers earthquake occurrence to be equally likely at each point within the zone and frequency is determined by the recurrence statistics developed for the zone as a whole. This is the Poisson spatial model. Alternatively, non-uniform patterns of seismicity observed in the historical record may be considered the best predictor for future earthquake occurrence within the broader zone (McGuire and Barnhard, 1981). To represent this interpretation, various types of spatial smoothing models may be applied, such as kernel

density estimation. A procedure of this type has been applied to construct the recent generation of national earthquake hazard maps (Frankel, 1995). This procedure results in a heterogeneous hazard function within any given zone. It is our view that the choice between the algorithms described above (or weighting) depends on the purpose of the hazard evaluation. If the goal is to characterize the hazard for an important facility with a relatively short economic life (say 150 years) for which a very low annual probability of exceedence for design parameters (say 10^{-4}) is desired, then a source zone characterization that mimics the observed patterns of historical seismicity should be given substantial weight in the hazard calculation. However, if the goal is to characterize seismic hazard for a much longer time span (say 10,000 years) with a reasonably low probability of exceedence, then the patterns of seismicity in the historical record may have little predictive value for occurrences on those time scales. In this case it would be appropriate to use a Poisson spatial model. It is our understanding that the performance assessors will be using results from the PSHA to judge the probability of occurrence of scenarios over 10,000-year, to 100,000-year, to multiple 100,000-year periods (SSC Workshop 5 discussion). Hence we have given a weight of 1.0 to the Poisson spatial algorithm for computation of hazard at this site.

4.0
FAULT DISPLACEMENT

4.1 INTRODUCTION

We characterize the potential for both principal and distributed fault displacement on seismogenic (block-bounding or primary) faults, and distributed faulting on five classes of secondary, nonseismogenic faults or fractures. We use generalized displacement patterns for normal faults derived from observed historical displacements. We apply the approach to characterize the potential for displacement at nine designated points within the Controlled Area at Yucca Mountain, but it can be used to evaluate the potential for displacements at any point. We do not specifically incorporate large-scale displacement patterns on the Yucca Mountain faults, specifically the Solitario Canyon fault (SC) or the Bow Ridge fault (BWR), the faults that bound the repository block. Instead, we rely on observed historical surface-rupturing on range-front faults larger than those at Yucca Mountain, related to earthquakes of M ~ 7.

There are two basic approaches for estimating the amount and timing of potential displacement on secondary faults (SSC Workshop 6). One approach is to derive all estimates from the secondary fault itself, based on its cumulative displacement, length, slip rate, or other parameters. This approach does not directly address the setting of the secondary fault, i.e., its distance to primary faults, whether it is one of many similar faults or exists alone in an otherwise unfractured block of rock, and so on; but rather assumes that these influences are reflected adequately in the fault parameters. The other approach is to examine the observed pattern of rupture in fault-bounded blocks and use this information to estimate potential displacement on distributed faults based on their position relative to principal fault rupture. This is the approach we adopted.

We consider the probability of fault displacement to be independent of depth. That is, we consider the displacement gradient between the repository level and the ground surface to be zero. Where the repository is near the surface, there is little error induced by this interpretation, because the distance over which slip would be attenuated is small. Where the repository is as much as 300 m below the surface, there is a possibility of displacement attenuation upward from the repository level to the ground surface. Whereas some data are available on slip gradients along strike in historical surface ruptures (e.g., McCalpin, 1996, p. 278, 289), few direct observations have been made on slip gradients in the dip direction during coseismic events. The observations of displacements in tunnels and mines beneath surface ruptures are too few on which to rely. Given this lack of data, our characterization of the potential for displacement applies equally to the ground surface and to the repository level (i.e., no attenuation in the dip direction).

Our approach for characterizing principal faulting hazard on seismogenic faults is based on the empirical distributions of along-strike displacement by Wheeler (1989) from the analysis of large Basin and Range earthquakes. We note that the displacement-along-strike curve for the SC fault (as described by A. Ramelli at SSC Workshop 5) is anomalous compared to historical Basin and Range ruptures, in that displacement is very high in the central 20 percent of the fault and very low elsewhere. We infer that the curve is so irregular because it only contains displacements from two faulting events; with additional events, the curve should smooth out to more resemble the Wheeler curve, or the smooth, quasi-parabolic curve of cumulative displacement along strike (J.C. Yount, SSC Workshop 6). We also note that

the most critical part of the curve is that closest to the repository, i.e., the northernmost 30 percent of the fault. In that reach the SC fault curve is almost identical to the Wheeler curve, both in mean value and upper and lower confidence limits. The rapid decrease in SC slip south of the maximum is inconsistent with other faults at Yucca Mountain, which generally increase in displacement southward. This clearly is not the case with the SC fault. The highest displacements on the SC fault occur after the Iron Ridge fault has branched off, rather than before, as one would expect if fault displacements were additive after two fault strands merged. If the SC fault displacement curve were typical of the long-term trend, Yucca Mountain would be three times higher in the vicinity of Trenches T1-T3 than elsewhere. However, the crest of Yucca Mountain does not show anomalously high elevations in the 2-km-long reach in the center. For all of these reasons, we do not use the displacements curve for the SC fault to predict the magnitude of future coseismic displacements along strike, but rather the Wheeler (1989) relationship.

Our characterization of distributed faulting rests on several interpretations about the mechanics of faulting. First, we assume that all distributed (induced) slip occurs during surface-rupturing earthquakes on primary (seismogenic) faults. It does not occur during the interseismic part of the cycle when strain is accumulating. We make this assumption because distributed faulting has been observed to occur during surface-rupturing earthquakes on normal faults. Conversely, distributed surface faulting (such as surface faulting on an intrabasin fault) without surface faulting on the adjacent primary basin-bounding fault is rare.

Secondly, we assume that during the interseismic part of the cycle, a crustal slab containing one (or more) secondary (nonseismogenic) faults in the hanging wall is strained elastically (the same is true for the foot wall). At the end of the seismic cycle, when the primary fault ruptures, the crustal rocks on either side of the fault recover through a combination of elastic rebound and inelastic deformation (fault slip) on secondary faults and discontinuities. We use the measured ground displacement profile from the 1983 Borah Peak, Idaho earthquake to characterize the variation of this displacement as a function of distance from the principal fault rupture and location in the hanging wall or foot wall of the rupture. We utilize the amplitude of this displacement profile to represent the maximum potential for ground displacement, either through elastic rebound of the rocks, or slip on secondary features, or a

combination of the two. The amount of displacement that occurs on a secondary fault, if it slips, is characterized as some fraction of this potential.

4.2 METHOD OF CHARACTERIZING THE POTENTIAL FOR FAULT DISPLACEMENT

Our method of characterizing potential fault displacement is described graphically by the logic trees shown on Figures ASM-16a and ASM-16b. We use slightly different methods for estimating the frequency and amount of slip on faults, depending on whether the fault is primary or secondary. Primary faults can experience displacement within 300 meters of the surface as principal fault rupture or as distributed fault rupture in response to principal rupture on other faults. Secondary faults can only experience distributed fault rupture.

4.2.1 Method for Principal Faulting

Figure ASM-16a shows the logic tree for characterizing the potential displacement on block-bounding, (primary) faults due to the occurrence of earthquakes on these faults. The characterization consists of the following steps.

4.2.1.1 Frequency of Potential Principal Faulting Events. The frequency of displacements occurring on a fault is estimated using the seismic source characterization developed in Section 3.0. The probability that principal faulting can occur is equal to the probability that the fault is seismogenic (see Section 3.4.1).

4.2.1.2 Probability of Principal Faulting Surface Displacement During Earthquakes. The probability that displacement will occur at or near the surface during an earthquake is computed using an empirical relationship between magnitude and the probability of surface rupture developed from the data presented in S. K. Pezzopane and T. E. Dawson (USGS, written communication, 1996). Figure ASM-17 shows these empirical relationships presented in SSC Workshop 5. Of the three regression curves in Figure ASM-17, we weight the leftmost curve (labeled 32 GB events) 0.5 and the rightmost curve (labeled 105 events EC) 0.5. (The equations defining these relationships are presented in Appendix H, Section H.4.1.) These weights reflect the fact that we have no clear preference for one extreme curve over another, and we wish to capture the full range of uncertainty. The probability that slip occurs at a point of interest on a fault, given that slip occurs near the surface, is computed by

randomizing the rupture along the fault. The length of the rupture is specified by the magnitude-rupture length relationships used in the ground motion hazard calculation.

4.2.1.3 Characterization of Displacement at a Point. The probability distribution for displacement occurring at a point of interest is computed in two steps. First, the maximum displacement on the primary fault is estimated using the Wells and Coppersmith (1994) relationship for maximum displacement (*MD*) as a function of earthquake magnitude. The variability in maximum displacement from event to event also is computed using the standard error for log(*MD*) found by Wells and Coppersmith (1994). The selected relationship is

$$\log(MD) = -5.46 + 0.82\mathbf{M}, \quad \sigma_{\log(MD)} = 0.42$$

Given a maximum displacement, we use the normalized relationships shown on Figure ASM-18 to obtain the distribution for displacement at any point on the fault rupture. Figure ASM-18 was developed using the normalized displacement distributions developed by Wheeler (1989). The data were smoothed by hand to produce curves symmetric about the midpoint of the rupture. The minimum and maximum curves on Figure ASM-18 are intended to represent low (~ 5%) and high (~95%) cumulative probabilities for the ratio of the displacement at a point to the maximum displacement. (Appendix H, Section H.3.1 presents a statistical distribution fit to these data.)

4.2.2 Method for Distributed Faulting

Figure ASM-16b shows the logic tree that characterizes the potential for distributed faulting on both primary and secondary faults and fractures. The approach consists of the following steps.

4.2.2.1 Probability Feature Can Slip. The first step in the characterization potential of the potential for distributed faulting is an evaluation of the likelihood faulting can occur on the feature of interest. This is the product of two probabilities, one based on the cumulative displacement category of the feature and one based on the strike of the feature.

Probability of distributed displacement as a function of fault displacement category. The probability of displacement depends on the cumulative displacement of the target feature. This interpretation is based on a conceptual model in which faults in extending crust evolve through time (e.g., Journal of Structural Geology, Special Issue on Fault Populations, 1996, v. 18, no. 2/3). In this model, many small faults are created during the initial phases of extension. As extension continues, some small faults coalesce to form larger faults. The larger faults become preferred loci of extension (due to their size and continuity), and thus accommodate larger displacements. With larger displacements, the fault gouge zone becomes better developed, lowering fault strength and encouraging an even greater concentration of displacement on these faults. In this progression, small-displacement faults are abandoned and larger-displacement faults accommodate more and more of the extensional strain budget.

Applying this model to Yucca Mountain implies that the smaller the displacement on a fault or fracture, the higher chance that it was abandoned in the early stages of Neogene extension and no longer experiences displacement. This concept accords with field observations by W. C. Day *et al.* (USGS, written communication, 1996b) that many fractures and small-displacement faults ceased to experience displacement between the deposition of the Tiva Canyon and Rainier Mesa tuffs. A corollary to this concept is that intact rock has a negligible probability of experiencing future fault displacement. From a mechanics standpoint, there are so many pre-existing fractures and faults in the Controlled Area that the formation of new fractures to accommodate extensional strain is not considered necessary.

We characterize the potential for distributed displacement on faults or fractures within six predefined classes of cumulative displacement (Table ASM-9). Listed in Table ASM-9 is the assessed probability that distributed faulting can occur for each class of feature. The probabilities in Table ASM-9 reflect our judgment that on the one hand, block-bounding faults (class 0) are certain to experience distributed displacement (having by definition experienced principal displacement), whereas fractures have a very small chance (P = 0.01) of experiencing future distributed displacement. The intermediate probability values for class 1-4 reflect our approximate linear subdivision between extreme probabilities of 0.01 and 1.0. These probabilities express the likelihood that there will ever be any future distributed displacement on this structure. This meaning of probability is meant to cover our estimates that

progressively smaller faults were created in an earlier stage of mechanical evolution of the crustal slab, and could be permanently abandoned now that larger, more continuous faults exist to accommodate displacement.

Probability as a function of fault/fracture orientation. Yucca Mountain faults that display evidence of Quaternary displacement all strike roughly north-south, an orientation that is compatible with the observed extension direction of approximately east-west (W. C. Day *et al.*, USGS, written communication, 1996b). Given this extension direction, distributed faults and fractures having north-south strikes are most favorably oriented to accommodate induced extension. H. L. McKague *et al.* (CNWRA, written communication, 1996) quantified the favorability of slip in the present stress field, termed slip tendency. We use slip tendency to make an estimate of the probability that induced slip can occur on a distributed fault or fracture. Based on the diminishing east-west component of displacement on faults having successively more east-west strikes, we define the probability of induced slip on a fault as the sine of the angle between its strike and east-west. Thus, for north-south-striking faults, the angle is 90 degrees, so P = 1; for N45W-striking faults, P = 0.87; and for east-west-striking faults, P = 0.

4.2.2.2 Frequency of Potential Distributed Faulting Events. Earthquakes that may induce distributed faulting can occur on any of the primary, block-bounding faults, or can be background earthquakes within the local areal source zone. Because seismicity rates for the areal source are considerably higher than for any specific fault source (see Section 3.4), we consider it critical to incorporate the effects from areal sources. Earthquake recurrence relationship for all of the sources are defined in Section 3.0.

4.2.2.3 Probability of Distributed Displacement on a Feature. The next step in the characterization of the potential for distributed faulting is an evaluation of the likelihood of faulting on the feature of interest due to the occurrence of an earthquake. This is the product of two probabilities, one based on whether the earthquake ruptures the surface on the primary fault and one based on the distance of the feature from the primary fault and the feature's location in the hanging wall or foot wall of the rupture.

Probability of secondary displacement as a function of whether surface rupture occurs. It is our interpretation that secondary faulting is only induced by surface-rupturing earthquakes. We make this assumption because: 1) most historical secondary faulting has been accompanied by surface rupture on the primary fault, and 2) the ground surface deformation data from the Borah Peak earthquake, which we use as a basis for estimating distributed faulting displacements reflects a surface-rupturing event.

The probability that an earthquake ruptures the surface, regardless of whether it occurs on a known primary fault, or on an unknown fault as a background earthquake, is a function of its magnitude. Therefore, we use the 32-event and 105-event curves from Pezzopane (as described in Sec. 4.2.1.2) to calculate the probability that a given primary earthquake will rupture the surface, and thus be able to induce distributed displacement.

Probability of distributed displacement as a function of distance to primary fault. The probability that distributed displacement will occur at a given distance from the principal rupture is assessed using an empirical relationship based on the density of distributed faulting observed for Basin and Range earthquakes. Figure ASM-19 shows the results of analysis by R.R. Youngs (presented at SSC Workshop 6) of distributed rupture patterns based on data presented in S. K. Pezzopane and T. E. Dawson (USGS, written communication, 1996). This figure shows the decreasing density of distributed faulting for historical normal faulting earthquakes with increasing distance from the primary fault. We believe that the ergodic substitution applies in this case, so that the probability of fault displacement through time on a distributed fault at a given distance from a primary fault is the same as the ratio of the area containing distributed faulting to the area containing no distributed faulting at that same distance. In other words, given enough time, the percentage of time that a given secondary fault ruptured in distributed slip would converge on the percentage of area that ruptures at that distance from the primary fault.

We use two assessments of the frequency of distributed rupture as a function of distance from the primary rupture, as shown on Figure ASM-19. The leftmost curve is an envelope of maximum frequency for earthquakes in the range of **M** 6.0 to 6.9; we weight this curve 0.6. Our slight preference for this curve over the other one is based on two considerations: (1) most of the estimated maximum earthquakes on Yucca Mountain faults are in the range of **M**

6.0 to 6.9 range, so we consider that magnitude range to be most appropriate; and (2) the maximum frequency values for this magnitude range define a relatively smooth trend that decreases with increasing distance from the primary rupture. We believe that the frequency of distributed displacement on a secondary fault should decrease with increasing distance to the seismogenic fault, based on our ergodic assumption described earlier, and the fact that for historical earthquakes, distributed faulting increases in density toward the primary fault (S. K. Pezzopane and T. E. Dawson, USGS, written communication, 1996).

We weight the right-most curve on Figure ASM-19 at 0.4, for the following reasons. First, Pezzopane (pers. comm., 1997) indicates that all the frequency values in his plot are minima, because: (1) the older points in the data set represent field reconnaissances that may have underestimated the extent of distributed faulting; and (2) although more recent investigations may be more thorough, they only record distributed faulting that broke to the surface, which is a minimum value for distributed faulting at depths as great as 300 m. Second, we wish this curve to represent the fact that the other curve is a minimum value. We accomplish this by drawing a curve parallel to the leftmost curve, through the maximum values plotted for **M** 7.0 to 7.9 earthquakes. We do not use the logistic regression fits of R.R. Youngs (presented at SSC Workshop 6), because they do not represent our interpretation that all plotted points are minimum values.

The relationships shown on Figure ASM-19 are dependent on the location of a feature within the hanging wall or foot wall of the principal rupture. This geometry is not known for earthquakes occurring within the regional source zone. Therefore, we consider it is equally likely that the point at which an assessment is made lies within the hanging wall or foot wall of the rupture.

4.2.2.4 Characterization of Distributed Displacement. The characterization of distributed displacement at a point on a feature is based on D/D_{max} defined for the principal rupture times a reduction factor (RF) that depends upon the distance and class of feature being considered. The approach is illustrated schematically on Figure ASM-20. Given the location of a point at which fault displacement hazard is being assessed with respect to a primary rupture, the distance to the rupture, x, and the location of the nearest point on the rupture, y, are defined. The distribution for displacement on the primary fault at location y, $[D(y)]$ is given by the

smoothed Wheeler curve (Figure ASM-18) once D_{max} has been specified. Two alternative approaches are used to define the values for *RF*, one based on what we term the across-strike secondary deformation (ASSD) method and one based on the relative cumulative offset on the earthquake source compared to the feature of interest.

Description of the ASSD Method. During historical normal faulting events, distributed faulting is larger and more frequent on the hanging wall near the seismogenic fault, and decreases away from the fault (S. K. Pezzopane and T. E. Dawson, USGS, written communication, 1996). The density of distributed faulting at a given distance from the fault is greater on the hanging wall than on the foot wall (Bob Smith presentation at SSC Workshop 6). This pattern is similar to the pattern of coseismic geodetic ground displacement observed following a normal faulting earthquake. We consider the amount of potential displacement on a distributed fault to be related to the amount of accumulated interseismic strain in the nearby crustal slab. This potential displacement is interpreted to have its maximum at the primary fault, where it is realized as the principal faulting displacement, and to decrease with distance from the principal rupture. This assumption lies at the heart of the ASSD method.

We first characterize the potential displacement, $DP(x)$, on secondary faults based on their distance perpendicular to the primary fault. This defines potential displacement along transects perpendicular to the seismogenic faults. $DP(x)$ is considered to be equal to or less than the predicted vertical coseismic geodetic displacement of the ground surface, which reflects the displacement of the strained crustal slab within 10 to 20 km of a seismogenic normal fault. We consider that potential (vertical) slip on any secondary fault must be equal to or smaller than the predicted vertical geodetic displacement, in order to avoid overcompensation of the elastic shape change accumulated during the previous earthquake deformation cycle.

To assess $DP(x)$ we use the geodetic profile from the 1983 Borah Peak earthquake, Figure ASM-21. We rescale the Borah Peak geodetic curve in both the vertical (z) and horizontal (x) directions. The vertical dimension is normalized by 1.44 m (the principal faulting displacement at the point of intersection of the Borah Peak geodetic profile with the fault trace). We expect the horizontal extent of distributed rupture to increase with increasing penetration of the

principal fault into the crust. Thus, the horizontal dimension is rescaled by the inverse of the ratio of the downdip extent of the primary earthquake compared to 16 km (downdip extent of the Borah Peak event). As a result, earthquakes larger than the Borah Peak earthquake will produce the same displacement potential at a greater distance from the principal rupture; earthquakes smaller than the Borah Peak earthquake will produce the same displacement potential at a smaller distance from the principal rupture.

The proportion of $DP(x)$ that is realized as distributed fault slip is difficult to estimate, thus we consider a wide distribution for defining the fraction of $DP(x)$ that is realized in distributed rupture on a single feature at the point of interest. This distribution is expressed as four discrete alternatives that are based on two considerations.

First, we consider it likely that better-developed faults accommodate a higher percentage of $DP(x)$ than less-developed faults, because they are more continuous, longer, and wider. As such, they have more cumulative displacement and better-developed fault gouge, thus weaker material properties in the fault zone, and less resistance to shear.

Secondly, there is a logarithmic increase in the number of progressively less-developed faults in any volume of rock (Nicol *et al.*, 1996). Most papers in the 1996 Journal of Structural Geology, Special Issue (v. 19, no. 2/3) cite a power law relationship between N (number of faults) and D_{cum} (the cumulative displacement on a fault), with an exponent of -0.7 to -0.8, or $\log(N) = C - 0.7 \times \log(D_{cum})$, where C is a constant. Thus, coseismic distributed faulting in the crustal slab can be accommodated by displacement on one well-developed fault, or on several less-developed faults.

Using the power law relationship given by Nicol *et al.* (1996), we compute the number of faults in all six fault classes when the number in any one class is known. For example, fault classes 0, 1, and 2 are typically mapped at the surface, but 3 through 5 are not. Thus, if we know that in a certain area there is one class 1 fault (D_{cum} = 35 m), we may predict that there are 2.2 faults that have D_{cum} = 11 m (class 2); 10.3 faults having D_{cum} = 1.25 m (class 3); and 28 faults having D_{cum} = 0.3 m (class 4). We then consider that $DP(x)$ can be partitioned among the classes of faults. We list in Table ASM-9 the expected number of faults in each class compared to one fault in class 0 with a cumulative displacement of ~100 m.

We define four possibilities for the partition of $DP(x)$ to define the displacement on an individual feature. These several approaches are necessary due to the way in which the problem of fault displacement characterization was posed by the Facilitation Team. They specified the existence and fault displacement class of the feature of interest at nine test points, but did not specify what displacement class or how many faults/fractures were in the near vicinity of the feature of interest. Our method assumes that if secondary displacement does in fact occur on the feature of interest (as determined by the preceding probability branches in the fault displacement logic tree), that it is likely that secondary displacement also occurs on some or all of the nearby faults. Thus, we desire to partition $DP(x)$ between the feature of interest and some/all of the surrounding faults, without knowing what class those other faults fall in, how many of them exist, and how far from the feature of interest they lie.

The first partition assumes that all of $DP(x)$ occurs on the fault/fracture of interest, $RF = DP(x)$. This partition defines the maximum possible distributed displacement that can occur on a feature in our method, because it assumes that: 1) 100% of $DP(x)$ is realized as distributed fault displacement, which is the limiting case, and 2) this entire displacement occurs only on the feature of interest, despite the fact that other faults and fractures may exist nearby. Given the limiting nature of this scenario we consider that it is an unlikely occurrence and assign it a probability of 5% that it occurs in an event.

The second partition assumes that 100% of $DP(x)$ occurs as distributed displacement in the vicinity of the feature of interest, but that $DP(x)$ is partitioned equally among the five classes of secondary faults. In other words, $RF = 0.2 \times DP(x)$ for each fault class. We consider this scenario to have a 20% likelihood of occurring in an event.

The third partition assumes that 100% of $DP(x)$ occurs as distributed displacement in the vicinity of the feature of interest, and that this displacement is partitioned among all faults in the same displacement class as the feature of interest. This assumption is made for the case that only faults similar to the feature of interest exist in the vicinity, so that other classes of faults may not share the displacement. Based on our examination of faults and fractures in the ESF, there are certainly some zones in the tunnel where most or all of the faults/fractures belong to the same displacement class. The number of faults in a particular class, N, is listed in Table

ASM-9. Thus, $RF = DP(x)/N$. We consider this scenario to have a 30% likelihood of occurring in an event.

The fourth partition assumes that 100% of $DP(x)$ occurs as distributed displacement, but the displacement is partitioned as 20% to each of the five secondary fault classes, and within each class, equally distributed among all faults in that class. Thus, $RF = 0.2 \times DP(x)/N$. We consider that is scenario is the most likely to occur (40%) because we consider it most plausible that, if distributed displacement does occur on the feature of interest, it would also occur on all of the nearly-identical faults/fractures nearby within the same fault displacement class.

The secondary displacement calculated for the feature of interest during a principal faulting event cannot exceed the cumulative displacement (D_{cum}) on that feature, but it may equal D_{cum}. The latter situation would arise if D_{cum} was all created in a single event, i.e., distributed faulting occurred only once during the lifetime of the secondary fault. Such a possibility cannot be ruled out. Therefore, we place an upper limit on the distributed displacement equal to D_{cum} of the feature.

The ASSD method utilizes the Borah Peak geodetic curve, which distinguishes between the hanging wall and foot wall consider to define $DP(x)$. When assessing the hazard from earthquakes occurring in the local source zone, we consider that it is equally likely that the feature of interest is located in the hanging wall or in the foot wall. We also consider that the assessment point is located normal to the midpoint of the earthquake rupture ($y/L = 0.5$).

Ratio of Cumulative Slips Approach. The alternative approach for assessing RF utilizes the ratio of the cumulative slip on the feature of interest to that on the fault where the principal rupture occurs. The concept of this approach is best explained in an simplified manner.

We consider the distributed faulting hazard at point 3 located on the Drill Hole Wash fault and assume for the moment that all of the cumulative displacement at point 3 resulted from the occurrence of characteristic earthquakes on only the Solitario canyon (SC) or Bow Ridge (BWR) faults. Because point 3 is located in the hanging wall of the BWR fault, it is likely that most of the distributed displacement resulted from earthquakes occurring on the BWR

fault because of the higher frequency of distributed rupture in the hanging wall (Figure ASM-19) and a larger displacement potential (Figure ASM-21). For the sake of illustration, we assume that 75% of the cumulative slip at point 3 occurred as a result of earthquakes occurring on the BWR fault and 25 % occurred as a result of earthquakes occurring on the SC fault. Over the lifetime of the BWR fault, n characteristic earthquakes have occurred, where $n = D_{cum}(\text{BWR})/D_{ch}(\text{BWR})$, where $D_{ch}(\text{BWR})$ is the displacement of the principal rupture of characteristic events on the fault. The fraction of these events that also produced distributed rupture at point 3 is $n \times P(\text{slip on 3}|\text{event on BWR})$, where $P(\text{slip on 3}|\text{event on BWR})$ is the probability of distributed slip at point 3 due to a characteristic earthquake on the BWR fault. Therefore, the expected displacement in a distributed slip at point 3 induced by a BWR characteristic earthquake is defined as the cumulative slip at point 3 due to earthquakes occurring on the BWR fault divided by the number of BWR events that induce distributed slip:

$$D(\text{point 3}) = 0.75 \times D_{cum}(\text{point 3})/[n \times P(\text{slip}|\text{event})]$$

The ratio of displacement on the feature at point 3 to displacement on the BWR fault defines the reduction factor, RF, and is given by:

$$RF(\text{BWR}) = \frac{D(\text{point 3})}{D_{ch}(\text{BWR})} = \frac{0.75 \times D_{cum}(\text{point 3})}{D_{cum}(\text{BWR}) \times P(\text{slip on 3}|\text{event on BWR})}$$

Similarly, the reduction factor for earthquakes occurring on the SC fault is given by:

$$RF(\text{SC}) = \frac{D(\text{point 3})}{D_{ch}(\text{SC})} = \frac{0.25 \times D_{cum}(\text{point 3})}{D_{cum}(\text{SC}) \times P(\text{slip on 3}|\text{event on SC})}$$

To apply this approach to the assessment of fault displacement hazard we must account for the distribution of earthquake magnitude that may occur on a seismic source and the contributions of multiple sources to the cumulative displacement at a point. To do this, we assume that the results of applying the ASSD approach provide a good assessment of the relative contribution of individual seismic sources to the distributed faulting displacement at the point of interest. As described in Section 4.2.2 of the main text, the displacement hazard curve can be used to

compute an effective slip rate that integrates the effects of all earthquakes occurring on all sources, designated as *TESR*. If a displacement hazard curve is computed for each source, then it can be used to compute the effective slip rate, *ESR*, due to earthquakes occurring on that source. Thus, the fraction of the cumulative slip induced by earthquakes on a particular source is estimated by the ratio of the effective slip rate for earthquakes on that source to the total effective slip rate. The result is that the reduction factor to apply to displacement on the BWR fault to estimated distributed displacement on the feature at point 3 is given by:

$$RF(\text{BWR}) = \frac{ESR(\text{BWR})}{TESR} \times \frac{D_{cum}(\text{point 3})}{D_{cum}(\text{BWR}) \times P(\text{slip on 3} \mid \text{event on BWR})}$$

The calculation of the effective slip rate using this approach still requires an evaluation of the probability that an earthquake on the primary fault will induce distributed rupture on the secondary fault. We assess this probability for the maximum event on the primary fault using the factors described in Section 4.2.2.3 because the maximum events on the various earthquake sources are expected to produce most of the distributed slip on any secondary feature.

Application of this method requires an assessment of the cumulative displacement on each of the seismic sources in the Yucca Mountain region. These values are as follows:

Fault	D_{cum} * (m)
	2600
BARE MOUNTAIN	
Bow Ridge	125
N. Crater Flat	00
S. Crater Flat	50
Fatigue Wash	72
Iron Ridge	215
Paintbrush Canyon	500
Solitario Canyon	700
Stagecoach Road	600
Windy Wash	500

*data from Table 4.2.1 in C. M. Menges and J. W. Whitney, (USGS, written communication, 1996a) and Chris Potter (personal communication, 1997).

As indicated in the logic tree shown on Figure ASM-16b, we assign a weights of 0.7 to the ASSD approach and 0.3 to the relative cumulative displacement approach. We favor the ASSD approach because it explicitly accounts for the effect of distance in the assessment of *RF* for each earthquake and does not assume that all of the faults have evolved in a parallel manner through time. It should be noted that only the ASSD approach can be used to assess the distributed faulting hazard from earthquakes occurring in the regional source zone because the cumulative slip on the sources is unknown. However, we do not believe that this is a significant detriment because these earthquakes are generally smaller than those occurring on the faults and are unlikely to produce principal faulting surface rupture. Thus their contribution to the total displacement hazard on a feature should be a small fraction of the total.

5.0
REFERENCES

Abers, G.A., 1991, Possible seismogenic shallow-dipping normal faults in the Woodlark-D'Entrecasteaux extensional province, Papua, New Guinea: Geology, v. 19, p.1205-1208.

Anderson, R.E., Bucknam, R.C. Crone, A.J., Haller, K.M., Machette, M.N., Personius, S.F., Barnhard, T.P., Cecil, M.J. and Dart, R.L., 1995a, Characterization of Quaternary and suspected Quaternary faults, regional studies, Nevada and California: U. S. Geological Survey Open-File Report 95-599, 56 p.

Anderson, R.E., Crone, A.J., Machette, M.N., Bradley, L., and Diehl, S.F., 1995b, Characterization of Quaternary and suspected Quaternary faults, Amargosa Area, Nevada and California: U. S. Geological Survey Open-File Report 95-613,41 p.

Arabasz, W.J., Pechmann, J.C., and Brown, E.D., 1992, Observational seismology and evaluation of earthquake hazards and risk in the Wasatch Front area, Utah, *in* Gori, P.L., and Hays, W.W., eds., Assessment of regional and earthquake hazards and risk along the Wasatch Front, Utah: U.S. Geological Survey Professional Paper 1500-D, p. D1-D36.

Beanland, S., and Clark, M.M., 1994, The Owens Valley Fault Zone, eastern California, and surface faulting associated with the 1872 earthquake: U. S. Geological Survey Bulletin 1994, 29 p. and 4 pls.

Brogan, G.E., Kellogg, L.S., Slemmons, D.B., and Terhune, C.L., 1991, Late Quaternary faulting along the Death Valley-Furnace Creek fault system, California and Nevada: U. S. Geological Survey Bulletin, map scale 1:62,500, 23 p., 4 pls.

Carr, W.J., 1990, Styles of extension in the Nevada test Site region, southern Walker Lane Belt; an integration of volcano-tectonic and detachment fault models, *in* Wernicke, B.P. (ed.), Basin and Range extensional tectonics at the latitude of Las Vegas, Nevada: Geological Society of America Memoir 176, p. 283-303.

Dohrenwend, J.C., Menges, C.M., Schell, B.A., and Morning, B.C., 1992a, Reconnaissance photogeologic map of young faults in the Las Vegas 1 x 2 quadrangle, Nevada, California, and Arizona: U. S. Geological Survey Miscellaneous Field Studies Map MF-2182, scale 1:250,000.

Dohrenwend, J. C., Schell, B. A., McKittrick, M. A., and Morning, B. C., 1992b, Reconnaissance photogeologic map of young faults in the Goldfield 1 x 2 degree quadrangle, Nevada and California: U. S. Geological Survey Miscellaneous Field Studies Map MF- 2183, scale 1:250,000.

Doser, D.I., 1987, The Ancash, Peru earthquake of 1946 November 10: evidence for low-angle normal faulting in the High Andes of Peru: Geophysical Journal of the Royal Astronomical Society, v. 91, p. 57-71.

Doser, D.I., and Smith, R.B., 1989, An assessment of source parameters of earthquakes in the Cordillera of the western United States: Bulletin of the Seismological Society of America, v. 79, p. 1393-1409.

Forsyth, D.W., 1992, Finite extension and low-angle normal faulting: Geology, v. 20, p. 27-30.

Frankel, A., 1995, Mapping seismic hazard in the central and eastern United States: Bulletin of the Seismological Society of America, v. 66, p. 8-21.

Fridrich, C., and Price, J., 1992, Tectonic framework of Crater Flat Basin, adjacent to Yucca Mountain, Nevada: A preliminary report: Geological Society of America, Abstracts with Programs, v. 24, no. 7, p. 189-190.

Gianella, V.P. and Callaghan, E., 1934, The earthquake of December 20, 1934 at Cedar Mountain, Nevada and its bearing on the genesis of Basin and Range structure: Journal of Geology, v. 42, p. 1-22.

Gomberg, J., 1991a, Seismicity and shear strain in the southern Great Basin of Nevada and California: Journal of Geophysical Research, v. 96, p. 16,383-16,399.

Gomberg, J., 1991b, Seismicity and detection/location threshold in the southern Great Basin Seismic Network, Journal Geophysical Research, v. 96, No. B10, P. 16401-16414.

Hackett, W.R., Jackson, S.M., and Smith, R.P., 1996, Paleoseismology of Volcanic Environments, *in* McCalpin, J.P., ed., Paleoseismology: San Diego, CA, Academic Press, Chapter 4.

Hardyman, R.F. and Oldow, J.S., 1991, Tertiary tectonic framework and Cenozoic history of the central Walker Lane, Nevada, *in* Raines, G.L., Lisle, R.E., Schafer, R.W., and Wilkinson, W.H., eds., Geology and ore deposits of the Great Basin: Geological Society of America, Nevada Symposium Proceedings, v. 1, p. 279-301.

Harmsen, S.C., and Bufe, C., 1991, Seismicity and focal mechanisms for the southern Great Basin of Nevada and California, 1987-1989: U.S. Geological Survey Open-File Report No. 91-572, 208 p.

Hunter, R.L., and Mann, C.J., eds., 1992, Techniques for determining probabilities of geologic events and processes: International Association for Mathematical Geology, Studies in Mathematical Geology, no. 4, Oxford University Press, Oxford, UK, 364 p.

Jackson, J.A., 1987, Active normal faulting and crustal extension, *in* Coward, M.P., Dewey, J.F., and Hancock, P.L. eds., Continental Extensional Tectonics: Geological Society of London Special Publication 28, p. 3-17.

Jackson, J.A., and White, N.J., 1989, Normal faulting in the upper continental crust; observations from regions of active extension: Journal of Structural Geology, v. 11, p. 15-36.

Johnson, R.A., and Loy, K.L., 1992, Seismic reflection evidence for seismogenic low-angle faulting in southeastern Arizona: Geology, v. 20, p. 597-600.

Mason, D.B. 1996, Earthquake magnitude potential of the intermountain seismic belt, USA, from surface-parameter scaling of late Quaternary faults: Bulletin of the Seismological Society of America, v. 86, n. 5, p. 1,487-1,506.

McCalpin, J.P., 1991, Quaternary surface-faulting earthquakes in the Overthrust Belt; did they occur on listric faults?: Geological Society of America, Abstracts with Programs, v.23, n. 7, p.140.

McCalpin, J.P., 1995, Frequency distribution of geologically determined slip rates for normal faults in the western USA: Bulletin of the Seismological Society of America, v. 85, n. 6, p. 1867-1872.

McCalpin, J.P. ed., 1996, Paleoseismology: Academic Press, New York, 583 p.

McGuire, R.K., 1985, Seismic hazard methodology for nuclear facilities in the eastern United States: EPRI Research Project Number P101-29, Dames and Moore, Golden, Colorado, Vol. 2, Appendix A.

McGuire, R.K., and Barnhard, T.P., 1981, Effects of temporal variations in seismicity on seismic hazard: Bulletin of the Seismological Society of America, v. 71, p. 321-334.

Nicol, A., Watterson, J., Walsh, J. J., and Childs, C., 1996, The shapes, major axis orientations and displacement patterns of fault surfaces: Journal of Structural Geology, v. 18, no. 2/3, p. 235-248.

Nicol, A., Walsh, J.J., Watterson, J., and Gillespie, P.A., 1996, Fault size distributions—are they really power-law?: Journal of Structural Geology, v. 18, no. 2/3, p. 191-198.

Nichols, W.D., 1987, Geohydrology of the unsaturated zone at the burial site for Low-Level Radioactive Waste near Beatty, Nye County, Nevada: U. S. Geological Survey Water-Supply Paper 2312.

Piety, L.A., 1995, Compilation of known and suspected Quaternary faults within 100 km of Yucca Mountain, Nevada and California: U. S. Geological Survey Open-File Report Number 94-112, 404 p.

Quade, J., Mifflin, M.D., Pratt, W.L., and Burkle, L., 1995, Fossil spring deposits in the southern Great Basin and their implications for changes in water-table levels near Yucca Mountain, Nevada during Quaternary time: Bulletin of the Geological Society of America, v. 107, n. 2, p. 213-230.

Reasenberg, P., 1985, Second order moment of central California seismicity, 1969-1982: Journal of Geophysical Research, v. 90, p. 5479-5495.

Reheis, M.C., 1992, Aerial photographic interpretation of lineaments and faults in late Cenozoic deposits in the Cactus Flat and Pahute Mesa 1:100,000 quadranges and the western parts of the Timpahute Range, Pahranagat Range,.Indian Springs and Las Vegas 1:100,000 quadrangles, Nevada: U. S. Geological Survey-Open File Report 92-193, scale 1:100,000, 14 p., 3 pls.

Reheis, M.C., and Noller, J.S., 1991, Aerial photographic interpretation of lineaments and faults in late Cenozoic deposits in the eastern part of Benton Range 1:100,000 quadrange and the Goldfield, Last Chance Range, Beatty, and Death Valley Junction 1:100,000 quadrangles, Nevada and California: U. S. Geological Survey-Open File Report 90-41, scale 1:100,000, 9 p., 4 pls.

Reheis, M.C., and Sawyer, T.L., 1997, Late Cenozoic history and slip rates of the Fish Lake Valley, Emigrant Peak, and Deep Springs fault zones, Nevada and California: Geological Society of America Bulletin, v. 109, n. 3, p. 280-299.

Richter, C.F., 1958, Elementary Seismology: William Freeman and Co., San Francisco, California, 300 p.

Rogers, A.M., Harmsen, S.C., Corbett, E.J., Preistly, K. and dePolo, D., 1991, The seismicity of Nevada and some adjacent parts of the Great Basin, *in* Slemmons, D.B. *et al.*, eds., Neotectonics of North America: Geological Society of America, Decade Map Volume, p. 153-184.

Savage, J.C., Lisowski, M., and Prescott, W.H., 1990, An apparent shear zone trending north-northwest across the Mojave Desert into Owens Valley, eastern California: Geophysical Research Letters, v. 17, p. 2113-2116.

Schwartz, D.P., and Coppersmith, K. J., 1984, Fault behavior and characteristic earthquakes: Examples from the Wasatch and San Andreas faults: Journal of Geophysical Research, v. 89, 5681-5698.

Schweickert, R.A., and Lahren, M.M., 1997, Strike-slip fault system in Amargosa Valley and Yucca Mountain, Nevada: Tectonophysics, v. 272, p. 25-41.

Sibson, R.H., 1985, A note on fault reactivation: Journal of Structural Geology, v. 7, p. 751-754.

Simonds, W.F., Whitney, J.W., Fox, K.F., Ramelli, A., Yount, J., Carr, M.D., Menges, C.M., Dickerson, R., and Scott, R.B., 1995, Map of fault activity of the Yucca Mountain area, Nye County, Nevada: U.S. Geological Survey Miscellaneous Investigations Series Map I-2520, scale 1:24,000.

Smith, K.D., Brune, J.N., Savage, M.K., Anooshepoor, R. and Sheehan, A.F., 1997, Main shock parameters and aftershock relocations of the 29 June 1992 Little Skull Mountain earthquake sequence: U.S. Geological Survey Circular on Yucca Mountain Tectonics, 42 p. (in press).

Smith, R. B., and Arabasz, W. J., 1992, Seismicity of the Intermountain Seismic Belt, *in* Slemmons, D. B., Engdahl, E.R., Zoback, M.D., and Blackwell, D.D., eds., Neotectonics of North America: Geological Society of America Decade Map, v. 1, Boulder, Colorado.

Stepp, C., 1972, Analysis of completeness of the earthquake sample in the Puget Sound area and its effects on statistical estimates of earthquake hazard, *in* Proceedings, First Microzonation Conference: Seattle, Washington, p. 987-909.

Stewart, J.H., 1987, Tectonics of the Walker Lane belt, western Great Basin—Mesozoic and Cenozoic deformation in a zone of shear, *in* Ernst, W.G., ed., Metamorphism and Crustal Evolution of the Western United States: Rubey Volume VII, Prentice-Hall Inc., New Jersey, p. 683-713.

Veniziano, D., and van Dyck, J., 1985, Statistical discrimination of "aftershocks" and their contribution to seismic hazard, Appendix A-4, *in* Seismic Hazard Methodology for Nuclear Facilities in the Eastern United States: EPRI Research Project No. P101-29, p. A121-A186.

von Seggern, D.H., and Brune, J.N., 1997, Seismicity in the southern Great Basin, 1968-1992, *in* Tectonic Characterization of Yucca Mountain—a Potential Geologic Repository for Nuclear Waste: Geological Society of America Special Volume (in press).

Wells, D.L., and Coppersmith, K.J., 1994, New empirical relationships among magnitude, rupture length, rupture width, rupture area, and surface displacement: Bulletin of the Seismological Society of America, v. 84, n. 4, p. 974-1002.

Wernicke, B., 1995, Low-angle normal faults and seismicity; a review: Journal of Geophysical Research, v. 100 (B10), p. 20,159-20,174.

Wesnousky, S.G., 1986, Quaternary faults and seismic hazards in California: Journal of Geophysical Research, v. 91, p. 12587-12632.

Wesnousky, S.G., Scholz, C.H., Shimazaki, K., and Matsuda, T., 1983, Earthquake frequency distribution and the mechanics of faulting: Journal of Geophysical Research, v. 88, p. 9331-9340.

Wheeler, R.L., 1989, Persistent segment boundaries on basin-range normal faults, *in* Schwartz, D.P. and Sibson, R.H. eds., Fault segmentation and controls of rupture initiation and termination: U.S. Geological Survey Open-File Report 89-315, p.432-444.

Wright, L.A., 1976, Late Cenozoic fault patterns and stress fields in the Great Basin and westward displacement of the Sierra Nevada block: Geology, v. 4, p. 489-494.

Youngs, R.R., and Coppersmith, K.J., 1985, Implications of fault slip rates and earthquake recurrence models to probabilistic seismic hazard estimates: Bulletin of the Seismological Society of America, v. 75, no. 4, p. 939-964.

Youngs, R.R., Swan, F.H. III, Power, M.S., Schwartz, D.P., and Green, R.K.,1987, Probabilistic analysis of earthquake ground shaking along the Wasatch Front, Utah, *in* W.W. Hays, and P.L. Gori, eds., Assessment of Regional Earthquake Hazards and Risk along the Wasatch Front: U. S. Geological Survey Open-File Report No. 87-585, v. II, p. 1-110.

Zhang, P., Ellis, M., Slemmons, D.B., and Mao, F., 1990, Right-lateral displacements and Holocene slip rate associated with prehistoric earthquakes along the southern Panamint Valley fault zone: implications for southern Basin and Range tectonics and coastal California deformation: Journal of Geophysical Research, v. 95, p. 4857-4872.

TABLE ASM-1
AVERAGE AND MAXIMUM DISPLACEMENTS FOR YUCCA MOUNTAIN FAULTS

Fault	Davg : Dpref Largest Event	Davg : Dpref All Events	Dmax : Largest Dpref	Dmax : Largest Dmax	Dmax : 2.59* Dpref Largest Event	Dmax : 2.59* Dpref All Events
Weights:	**0.5**	**0.5**	**0.25**	**0.5**	**0.125**	**0.125**
Bare Mountain (BM)	150	127	150	300	389	329
Bow Ridge (BWR)	44	24	44	80	114	62
N. Crater Flat (NCF)	50	47	50	50	130	122
S. Crater Flat (SCF)	13	20	20	32	34	52
Fatigue Wash (FW)	105	61	105	105	272	158
Iron Ridge (IR)	100	80	100	130	260	208
Paintbrush Canyon/ Stagecoach Road (SR-PBC)	167	51	167	205	433	132
Solitario Canyon (SC)	75	54	120	140	195	140
Windy Wash (WW)	58	44	88	98	150	114
Rock Valley (RV)	362	291	362	451	940	755

* Data was taken from all trenches, displacements are in cm.

TABLE ASM-2
SURFACE RUPTURE LENGTHS FOR YUCCA MOUNTAIN FAULTS

Fault	Minimum Length (km)	Preferred Length (km)	Maximum Length (km)
Weights:	**0.1**	**0.6**	**0.3**
Bare Mountain	17.5	20.6	24
Bow Ridge	6.7	7.6	9.4
N. Crater Flat	10.6	11.6	15.1
S. Crater Flat	6.1	7.8	8.8
Fatigue Wash	6.6	12.5	15.2
Iron Ridge	5.5	8.5	9.2
Paintbrush Canyon/ Stagecoach Road	18.0	24.0	28.5
Solitario Canyon	11.3	18.7	20.9
Windy Wash	15.6	21.6	24.6

TABLE ASM-3
WEIGHTING CRITERIA FOR MAXIMUM MAGNITUDES FOR YUCCA MOUNTAIN FAULTS

Fault	Msrl	Mra	Mmas	Mdmax	Mdavg
Bare Mountian	0.4	0.1	0.2	0.1	0.2
Bow Ridge	0.45	0.1	0.3	0.15	0
N. Crater Flat	0.3	0.2	0.3	0.2	0
S. Crater Flat	0.3	0.1	0.3	0.15	0.15
Fatigue Wash	0.35	0.25	0.3	0.1	0
Iron Ridge	0.4	0.2	0.2	0.2	0
Paintbrush Canyon/ Stagecoach Road	0.3	0.15	0.3	0.1	0.15
Solitario Canyon	0.3	0.1	0.3	0.15	0.15
Windy Wash	0.3	0.1	0.3	0.15	0.15

Methods: Msrl—surface rupture length (Wells and Coppersmith, 1994)
Mra—rupture area (Wells and Coppersmith, 1994)
Mmas—surface rupture length*displacement (Mason, 1996)
Mdmax—maximum displacement (Wells and Coppersmith, 1994)
Mdavg—average displacement (Wells and Coppersmith, 1994)

TABLE ASM-4
SLIP RATES FOR YUCCA MOUNTAIN FAULTS

Fault	20-percentile (mm/yr)	Median (mm/yr)	80-percentile (mm/yr)
Weights:	**0.2**	**0.6**	**0.2**
Bare Mountain	0.008	0.025	0.07
Bow Ridge	0.0008	0.002	0.0047
N. Crater Flat	0.0011	0.0025	0.0048
S. Crater Flat	0.001	0.0024	0.0047
Fatigue Wash	0.0038	0.009	0.0162
Iron Ridge	0.0015	0.0036	0.0068
Paintbrush Canyon/ Stagecoach Road	0.0065	0.016	0.029
Solitario Canyon	0.005	0.0125	0.024
Windy Wash	0.003	0.007	0.0128

TABLE ASM-5
RECURRENCE FOR YUCCA MOUNTAIN FAULTS

Fault	20-percentile (kyr)	Median (kyr)	80-percentile (kyr)
Weights:	**0.2**	**0.6**	**0.2**
Bare Mountain	42	87	143
Bow Ridge	71	120	188
N. Crater Flat	135	212	330
S. Crater Flat	65	107	165
Fatigue Wash	99	161	249
Iron Ridge	83	137	220
Paintbrush Canyon/ Stagecoach Road	17	27	42
Solitario Canyon	31	51	78
Windy Wash	31	50	79

TABLE ASM-6
REGIONAL FAULT DATA
(Page 1 of 2)

No.	FAULT [1]	MAP DESIGNATION	CLOSEST DIST. TO SITE [2] (km)	SLIP RATE (SR) [3] (mm/yr)			RECURRENCE INTERVAL (RI) [4] (yr)			SURFACE RUPTURE LENGTH (SRL) [5] (km)			TYPE [6]	DIP (DEG./ DIRECTION)
				MINIMUM	PREFERRED	MAXIMUM	MINIMUM	PREFERRED	MAXIMUM	MINIMUM	PREFERRED	MAXIMUM		
1	*Carrara?*	*H95*	15 DBS*	0.013 (0.2)	0.05 (0.6)	0.12 (0.2)	10000 (0.2)	19000 (0.6)	69000 (0.2)	10 (0.1) 10 (0.5)	20 (0.8) 20 (0.5)	42 (0.1)	SS	60-90/SW
2	Mine Mountain	MM	19 P1	0.006 (0.33)	0.03 (0.34)	0.06 (0.33)	20000 (0.33)	39000 (0.34)	146000 (0.33)	10 (0.5)	20 (0.5)		SS	VERT/SW
3	Wahmonie	WAH	22 P1	0.01 (0.33)	0.04 (0.34)	0.08 (0.33)	20000 (0.33)	39000 (0.34)	146000 (0.33)		14.5 (1.0)		0S	?/SE
4	*Ash Meadows*	*AM*	22 DBS	0.01 (0.2)	0.02 (0.6)	0.03 (0.2)	10000 (0.2)	35000 (0.5)	128000 (0.3)	10 (0.1)	38 (0.8)	40 (0.1)	N	60/W
5	*Rock Valley*	*RV*	25 Ch 4.13	0.02 (0.2)	0.06 (0.6)	0.09 (0.2)	34325 (0.2)	58333 (0.6)	175000 (0.2)	32.6 (0.2)	62.1 (0.6)	72 (0.2)	SS	VERT
6	*W Specter Range*	*WSR*	28 DBS	0.004 (0.3)	0.01 (0.4)	0.02 (0.3)	10000 (0.1)	25000 (0.6)	>128000 (0.3)	18 (0.8)		25 (0.2)	N	60/W
7	Cane Spring	CS	26 P1	0.007 (0.33)	0.03 (0.34)	0.07 (0.33)	20000 (0.33)	39000 (0.34)	146000 (0.33)	21 (0.5)		26 (0.5)	SS	VERT
8	*Amargosa River*	*AR*	34 DBS	0.01 (0.2)	0.05 (0.6)	0.09 (0.2)	10000 (0.1)	69000 (0.6)	128000 (0.3)	12.4 (0.2)	24.8 (0.6)	48 (0.2)	SS	VERT
9	Yucca Lake	YCL	36 P1	0.002 (0.33)	0.02 (0.34)	0.034 (0.33)	20000 (0.33)	39000 (0.34)	146000 (0.33)	16.3 (0.5)		20.6 (0.5)	SS?	VERT/?
10	Eleana Range	ER	37 P1	0.00006 (0.33)	0.00024 (0.34)	0.0003 (0.33)	20000 (0.33)	39000 (0.34)	146000 (0.33)	10.6 (0.5)		12.7 (0.5)	N	60/E
11	*E Specter Range*	*ESR*	37 DBS	0.004 (0.33)	0.012 (0.34)	0.021 (0.33)	10000 (0.33)	25000 (0.34)	128000 (0.33)	9 (0.5)		15 (0.5)	N	60/E
12	Yucca Fault	YC	40 P1	0.008 (0.33)	0.04 (0.34)	0.08 (0.33)	20000 (0.33)	39000 (0.34)	146000 (0.33)	23 (0.5)		33 (0.5)	SS?	VERT/?
13	*W Spring Mountains*	*WSM*	45 DBS	0.02 (0.2)	0.05 (0.6)	0.07 (0.2)	20000 (0.2)	69000 (0.6)	128000 (0.2)	14.6 (0.2)	43.5 (0.6)	50 (0.2)	N	60/W
14	*Furnace Creek*	*FC*	52 DBS	4 (0.2)	5 (0.6)	8 (0.2)	600 (0.2)	700 (0.6)	800 (0.2)	70 (0.2)	105 (0.6)	120 (0.2)	SS	VERT
15	*E Death Valley*	*EDV*	52 P1	3.46 (0.2)	4.62 (0.6)	5.77 (0.2)	500 (0.2)	875 (0.6)	1000 (0.2)	34 (0.2)	60 (0.6)	75 (0.2)	N	60/W
16	*Belted Range*	*BLR*	55 P1	0.02 (0.33)	0.04 (0.34)	0.1 (0.33)	20000 (0.33)	39000 (0.34)	69000 (0.33)	21 (0.6)		49 (0.4)	N	60/W
17	*M Death Valley*	*MDV*	57 DBS	1 (0.2)	2 (0.6)	3 (0.2)	1000 (0.2)	2000 (0.6)	5000 (0.2)	32 (0.2)	60 (0.6)	72 (0.2)	SS	VERT
18	Grapevine	GV	58 P1	0.003 (0.33)	0.01 (0.34)	0.02 (0.33)	20000 (0.33)	39000 (0.34)	146000 (0.33)		29 (1.0)		N	60/W
19	W Death Valley	WDV	61 DBS	0.009 (0.33)	0.05 (0.34)	0.16 (0.33)	20000 (0.33)	39000 (0.34)	146000 (0.33)	25 (0.3)	39 (0.5)	62 (0.2)	N	60/E
20	Emigrant/Towne Pass	EM-TP	<65 DBS	0.003 (0.33)	0.01 (0.34)	0.03 (0.33)	10000 (0.33)	20000 (0.34)	69000 (0.33)	14.6 (0.2)	17 (0.6)	47 (0.2)	N	60/NW
21	*N Pahrump-Stewart Valley*	*PRP*	69 DBS	0.03 (0.2)	0.06 (0.6)	0.14 (0.2)	10000 (0.2)	39000 (0.6)	69000 (0.2)	20 (0.5)		40 (0.5)	SS, OS?	VERT/?
22	*W Pintwater Range*	*WPR*	76 P1	0.005 (0.2)	0.01 (0.6)	0.06 (0.2)	10000 (0.33)	39000 (0.34)	69000 (0.33)	18 (0.33)	37 (0.34)	56 (0.33)	N	60/W
23	*Panamint Valley-Hunter Mountain*	*PAN-HM*	95 P1	1.57 (0.1)	2.36 (0.8)	3.15 (0.1)	700 (0.1)	1610 (0.8)	2360 (0.1)	40 (0.2)	70 (0.6)	120 (0.2)	SS	VERT
24	*S Pahrump-Stateline*	*SPRP*	107 DBS	0.002 (0.33)	0.05 (0.34)	0.1 (0.33)	20000 (0.2.)	39000 (0.6)	69000 (0.2)	31 (0.5)		65 (0.5)	OS	60?/W

TABLE ASM-6
(Page 2 of 2

Notes for Table ASM-6:

1 Fault number, name, and map designation (Figure ASM-9). The 15 faults with names shown in *italic font* have substantial field data, or correlate with faults that have substantial field data, for estimating slip rates (SR), recurrence intervals (RI), and approximate surface rupture length (SRL). The 9 faults with names shown with normal font have sparse characterization data. Data and observations supporting the characterization of regional fault sources are provided in Appendix ASM-6.

2 Approximate distance from Yucca Mountain; from Piety, 1995 (P1), or observations of D.B. Slemmons (DBS).

3 Slip rates for well studied (*italic font*) faults generally are based on paleoseismic data as reported in available literature (see references cited on Piety, 1995). Slip rates for other faults (normal font) are estimated from SRL data using the approach described in Section 3.5.3.1.

4 Field observations of historical Basin and Range surface faulting for events of Mw> 6.2, YM trench data and personal observations of southern Nevada faults show that more than 90 percent of Quaternary scarps are formed by recurrent events, generally having similar magnitudes and displacements, so nearly all of the tabulated faults are assumed to reflect recurrent activity. Recurrence interval (RI) for well studied faults (*italic font*) are based on references in Piety (1995) or personal observations. They are considered to have fixed age values that show the range of uncertainty; for faults that have a better database, a preferred value is given. The assigned weights are 0.2 for the extreme values and 0.6 for the preferred value. Recurrence intervals for other faults are estimated using the approach described in Section 3.5.4 in which an assumed number of surface rupturing earthquakes (3) is represented by the scarps in middle to late Pleistocene surfaces that are estimated to be middle to late Pleistocene in age (equal weight assigned to ages of 69 ka, 128 ka, and 449 ka) and have recurrence intervals estimated at 20, 39, and 146 kyr, respectively.

5 Surface rupture length (SRL). The maximum SRL is generally limited by connections on strike to other faults, major irregularities at the ends of rupture zones, or to terminations or truncations by other faults. The length is approximately expressed by the minimum, preferred, and maximum SRL interpreted from the pattern of the 24 faults and character and size of the surface rupture patterns from historical events in the Basin and Range Province. The lengths include a minimum of about 10 km, and a maximum of 40-75 km, which is within the range of longer historical surface faulting events for normal faults in the Basin and Range Province. Faults with special relationships (e.g., having lengths that appear to be controlled by truncations or connections with other faults) generally have only one, preferred SRL. Only one value is given for cases in which the length is supported by one map, generally Piety (1995).

6 SS = strike slip, OS = oblique slip, N = normal.

7 A high probability (0.85) is assigned to the Carrara fault being seismogenic based on the evidence summarized in Appendix ASM-6. However, because the fault has not been thoroughly characterized, some probability (0.15) is given to the fault being non-seismogenic. Two alternative total lengths of 20 km and 42 km are given equal weight in the source model.

TABLE ASM-7
RATIO OF AVERAGE TO MAXIMUM DISPLACEMENT

Worker	Number Of Events	Ad/Md Ratio	Range In Values
W&C (1994)	56, all fault types	0.5	0.2-0.8
Mason (1996)	15 normal faulting events using data from W&C (1996)	0.42	0.2-0.8
Mason (1996)	3 Basin and Range events	0.33	0.3-0.6
Slemmons, in preparation	5 Basin and Range events	0.39	
Slemmons, in preparation	15, all fault types	0.37	0.2-
Strom & Nikonov, unpublished manuscript	10 normal faulting events	0.38	0.21-0.58, standard deviation = 0.11

TABLE ASM-8
INFERRED NUMBER OF EVENTS

Seismic Source	Inferred Number Of Events	Data
Ash Meadows	2	Anderson *et al.*, (1995b)
Bare Mountain	Ca. 4	USGS (written communication, 1996), Anderson (SSC Workshop Presentation)
Belted Range	4 or possibly 5, using 1-1.5m maximum per event and SO up to 4.9 m. The anomalous value of 11.3 is assumed to be an older surface.	Anderson (1995a)
East Nopah	2 or 3	Anderson *et al.* (1995a) and DBS photographs
Kawitch Range	2, profile 2 appears to be on an older, but less than 100 ka surface.	Anderson *et al.* (1995a)
West Spring Mountains	3-5	
West Specter Range	2	Anderson *et al.* (1995a)

Average=20.7/7=~3

TABLE ASM-9
FAULT CLASSES FOR DISPLACEMENT POTENTIAL.

Class	Description	Seismogenic ?	Cumulative Displacement	Probability of Slip	Number of Feature, *N*
0	block-bounding (primary)	yes	>50 m	1.0	1
1	NW-trending (secondary)	no	20-50 m	0.75	2
2	Larger Intrablock (secondary)	no	2-20 m	0.5	4.4
3	Smaller Intrablock (secondary)	no	0.5-2 m	0.25	20.6
4	Small shear (secondary)	no	0.1-0.5 m	0.05	56
5	Fracture (secondary)	no	<<0.1 m	0.01	1000

Depth of BD Transition Or Seismic Crustal Thickness	*Detachment Exists*	*Buried SS Exists*	*Depth to Detachment*	*Detachment Seismogenic*	*Buried SS Seismogenic*	*Sources*

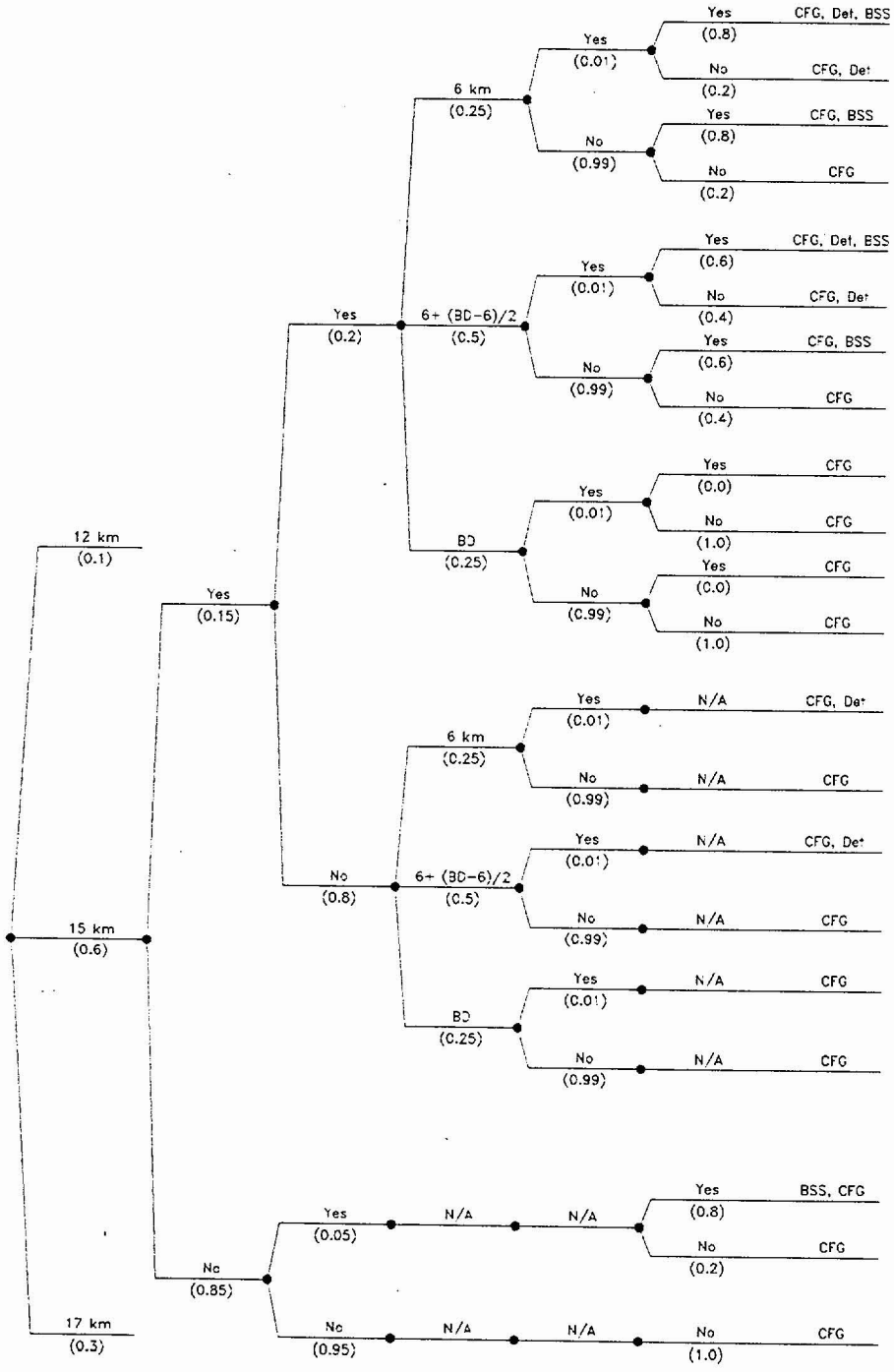

Figure ASM-1 Logic tree for local sources

Depth of Brittle Crust (BDT)	*Detachment Exists?*	*Depth of Detachment*	*Detachment Seismogenic*	*Detachment Geometry (area) (km^2)*

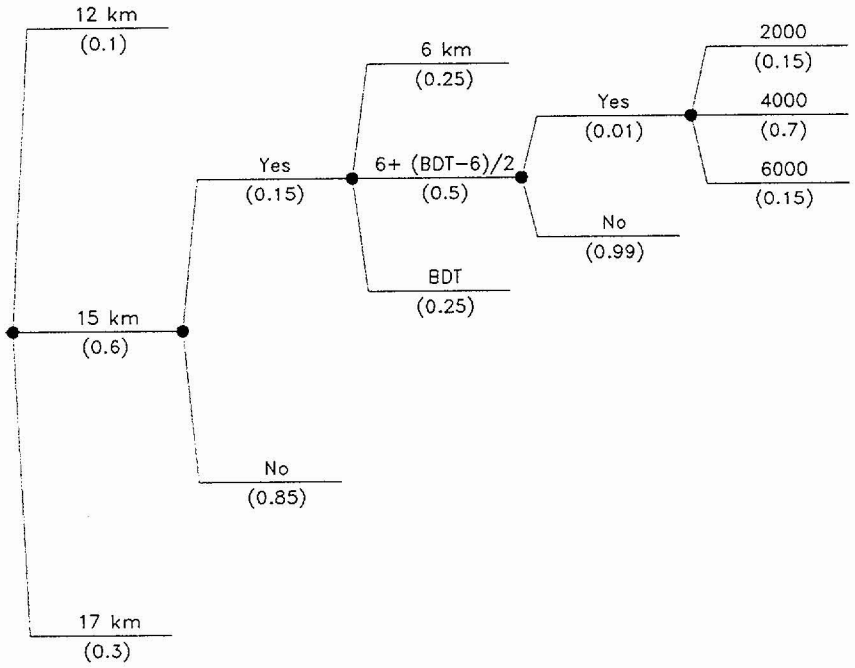

Figure ASM-2 Details of logic tree for detachment model

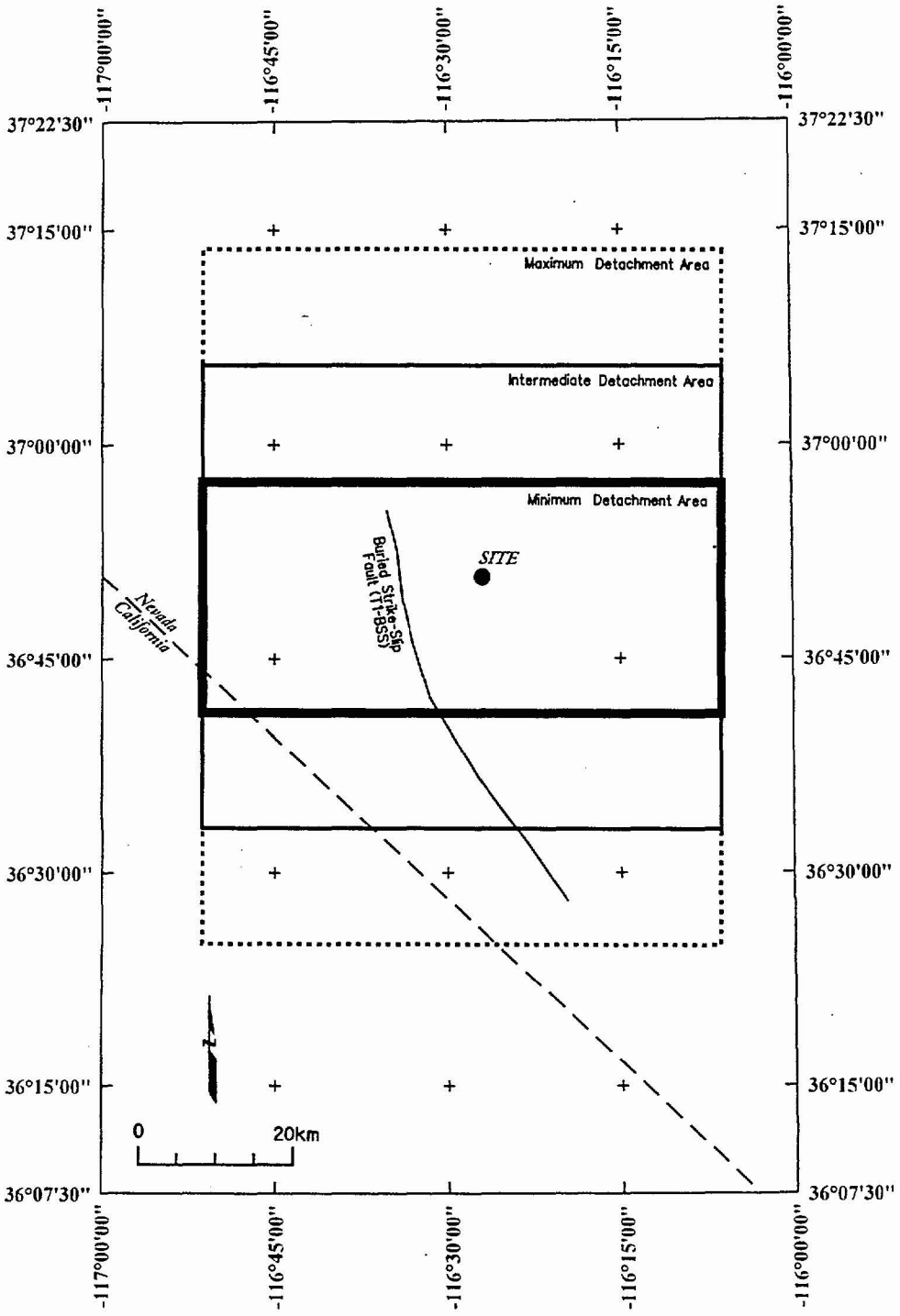

Figure ASM-3 Map showing hypothetical buried strike-slip fault and detachment fault in the vicinity of Yucca Mountain included in the seismic source model

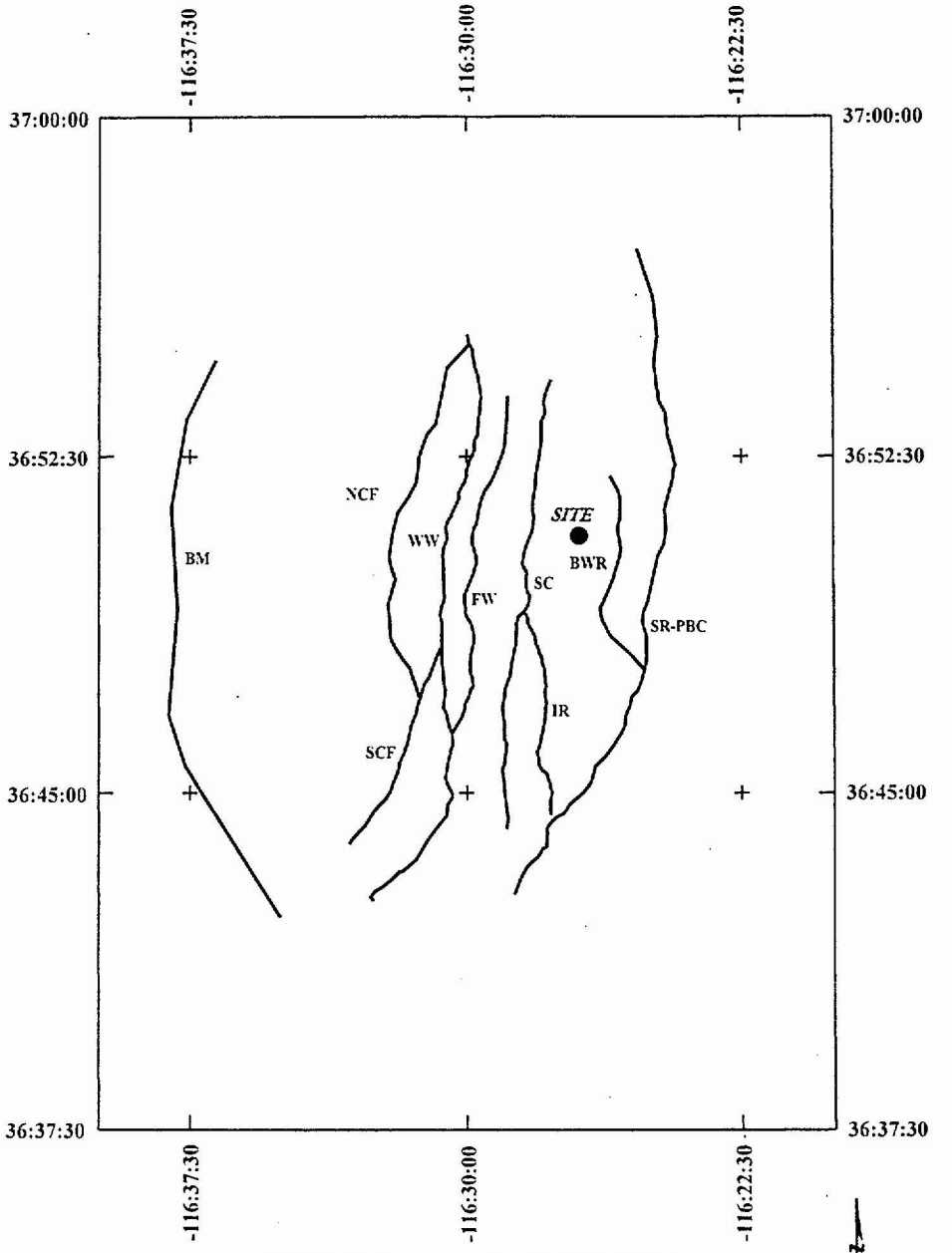

Figure ASM-4 Map showing local fault sources included in the seismic source model

h:\prj\yucca_mt\dgn\1097\plate_t1_lcl_fault.dgn 27-OCT-1997 15:13

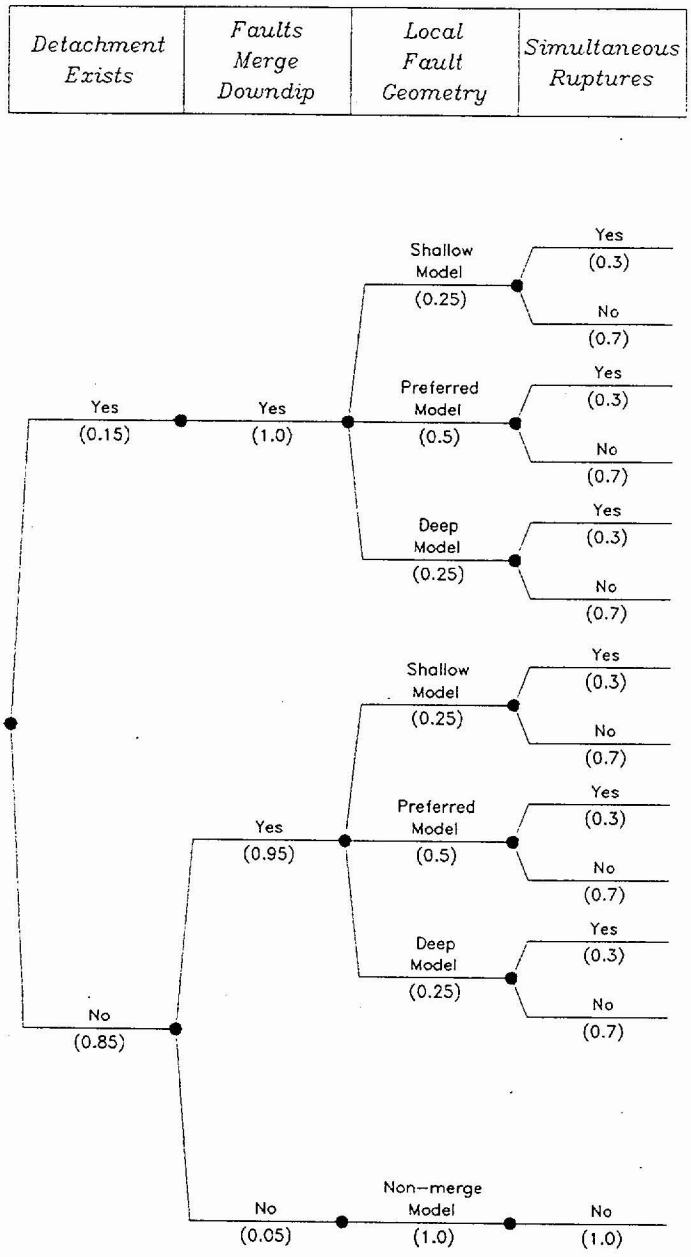

Figure ASM-5 Logic tree for Crater Flat group (CFG) behavior

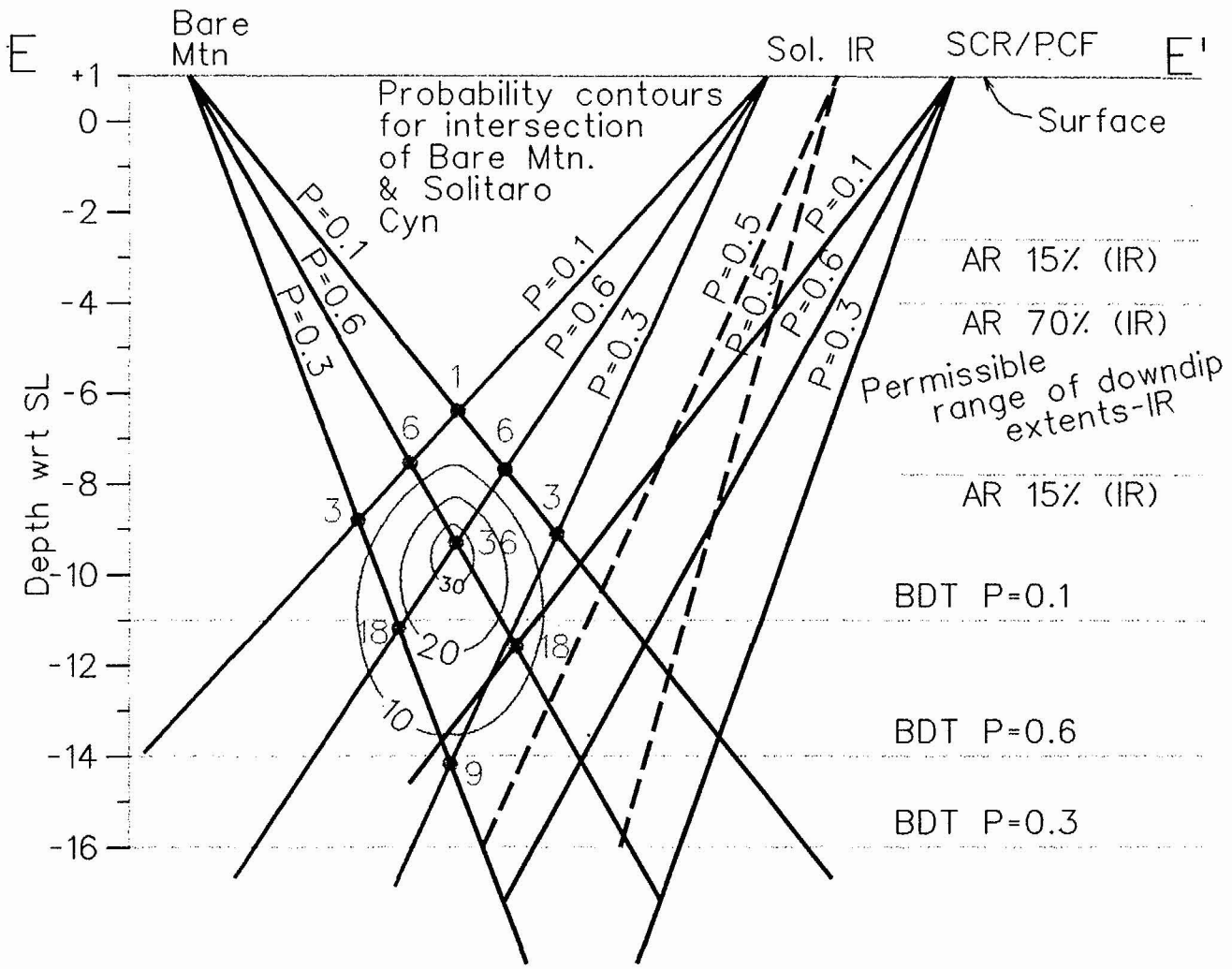

Figure ASM-6 Schematic of method used to develop downdip geometries of local faults

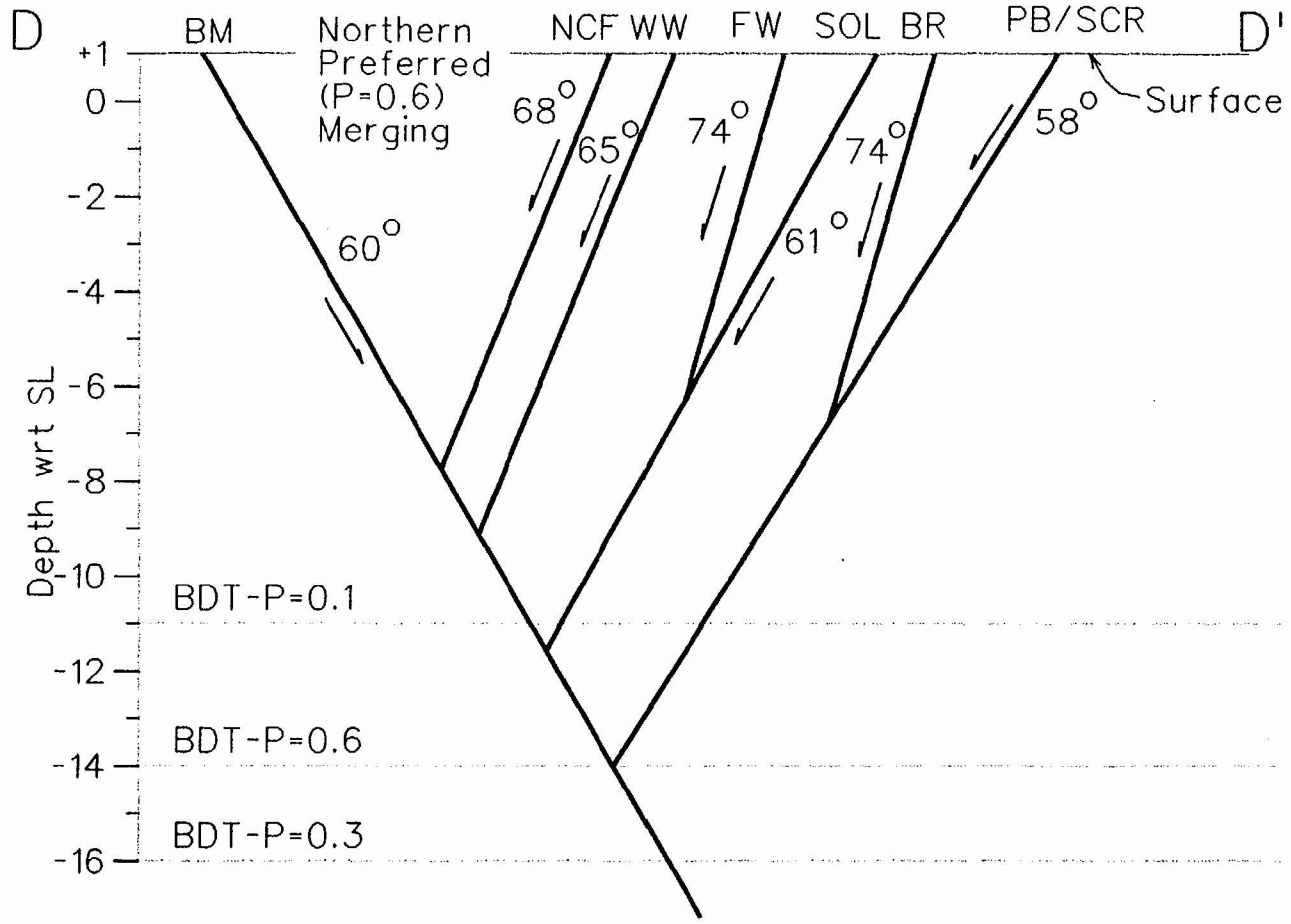

Figure ASM-7a Schematic cross section of preferred merging geometry, northern transect

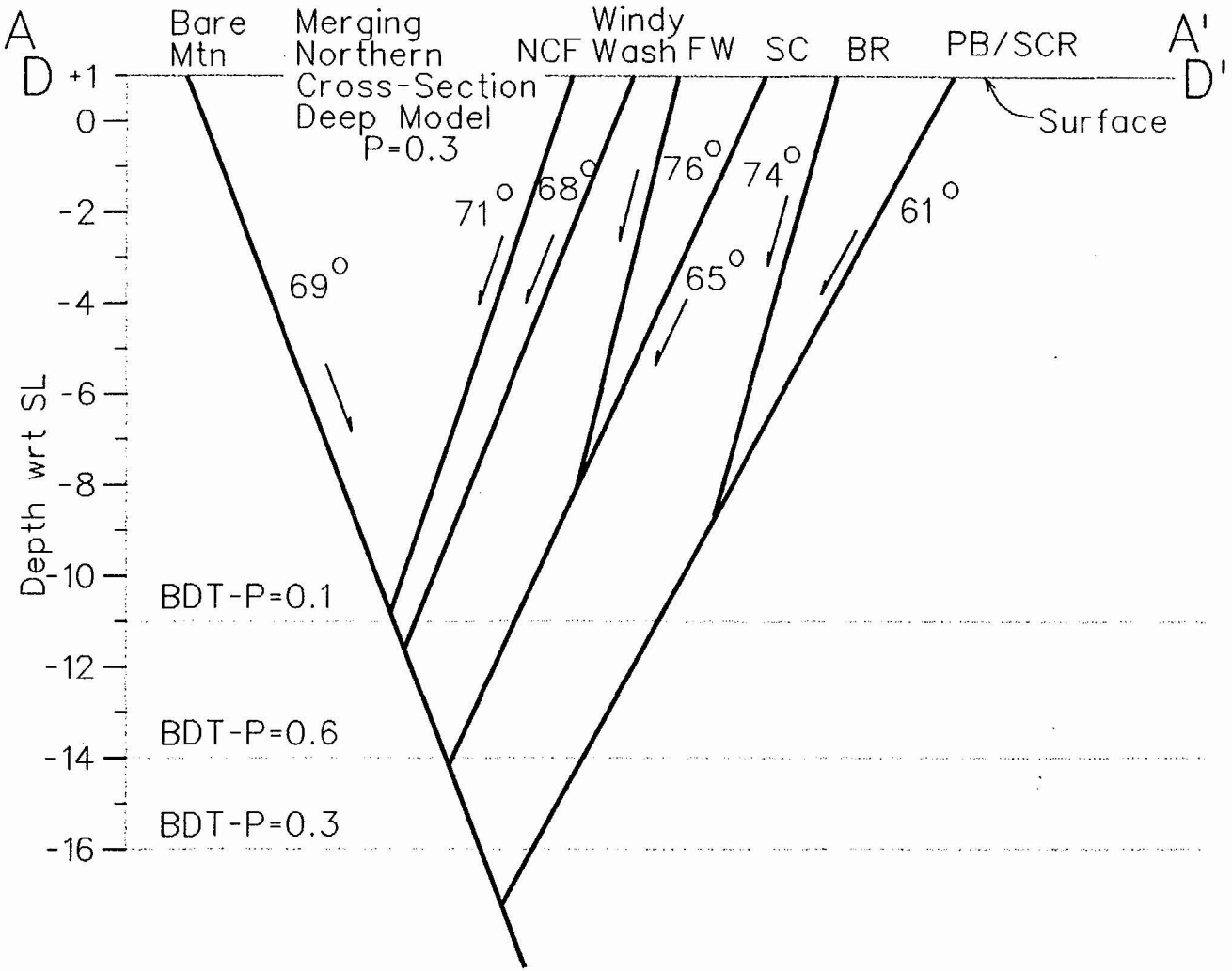

Figure ASM-7b Schematic cross-section of deep, merging geometry. Depth of secondary faults constrained by aspect ratio

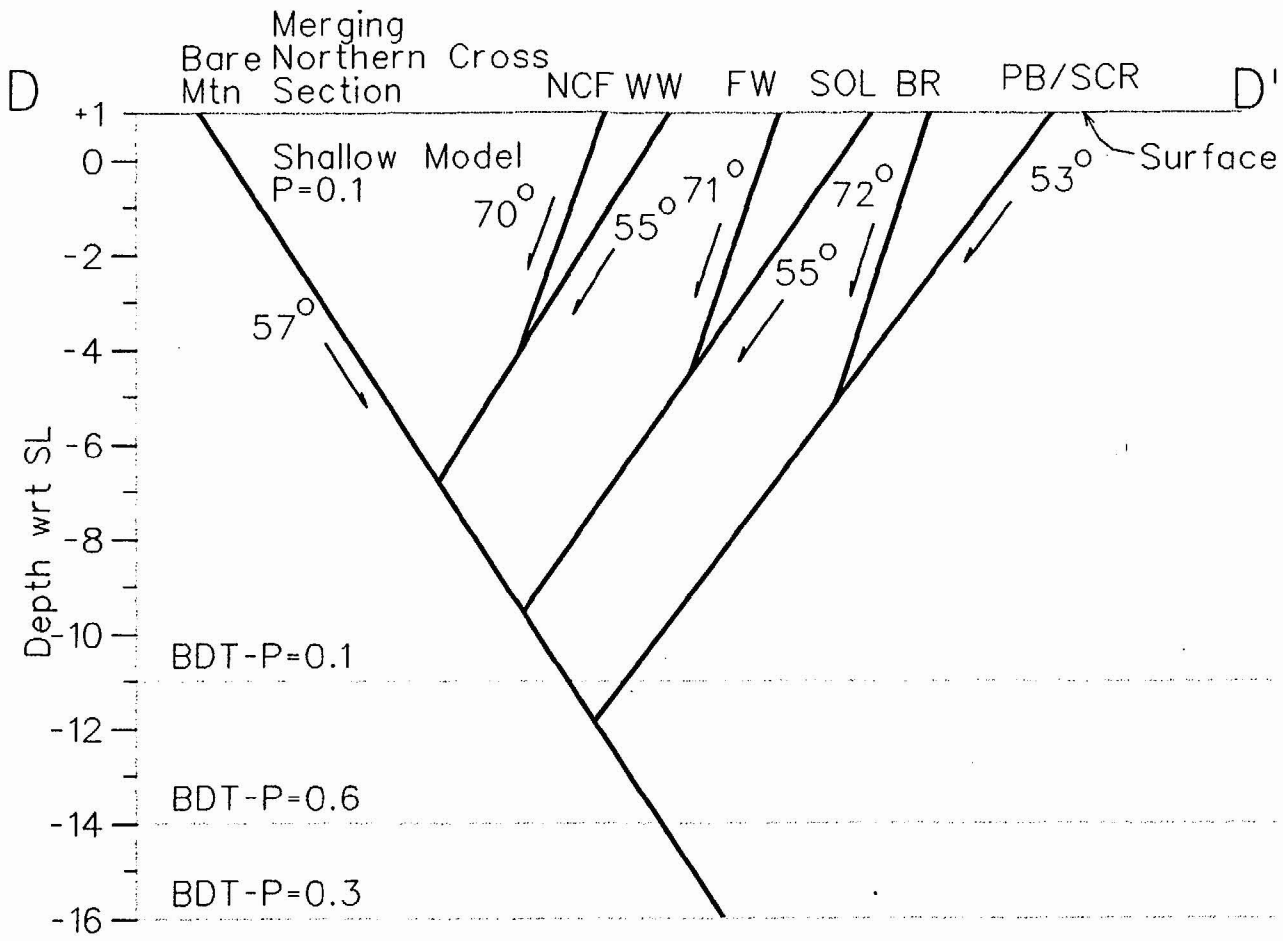

Figure ASM-7c Schematic cross-section of shallow, merging geometry, northern transect. Depth of secondary faults constrained by aspect ratio

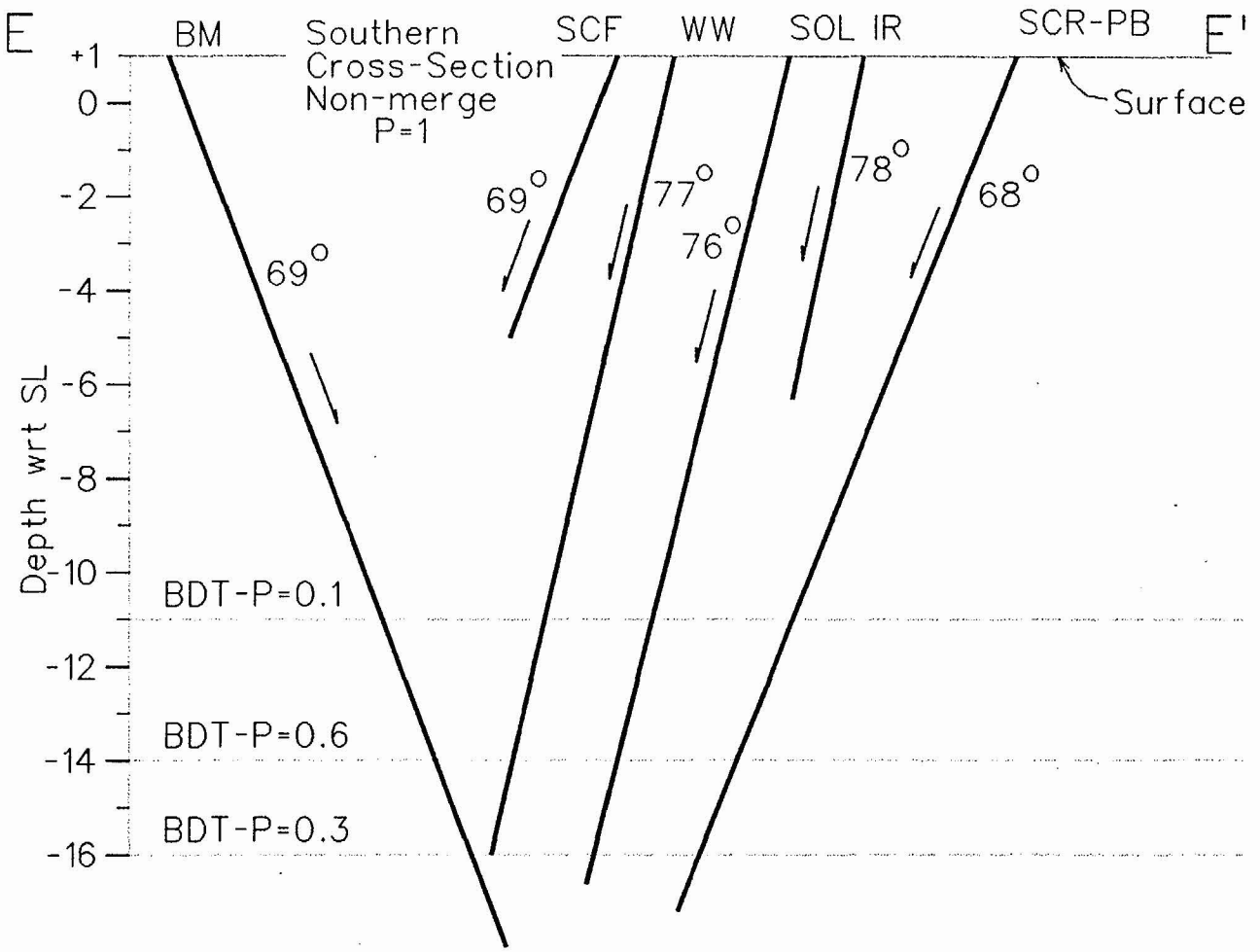

Figure ASM-7d Schematic cross-section of non-merging geometry. Depth of secondary faults constrained by aspect ratio

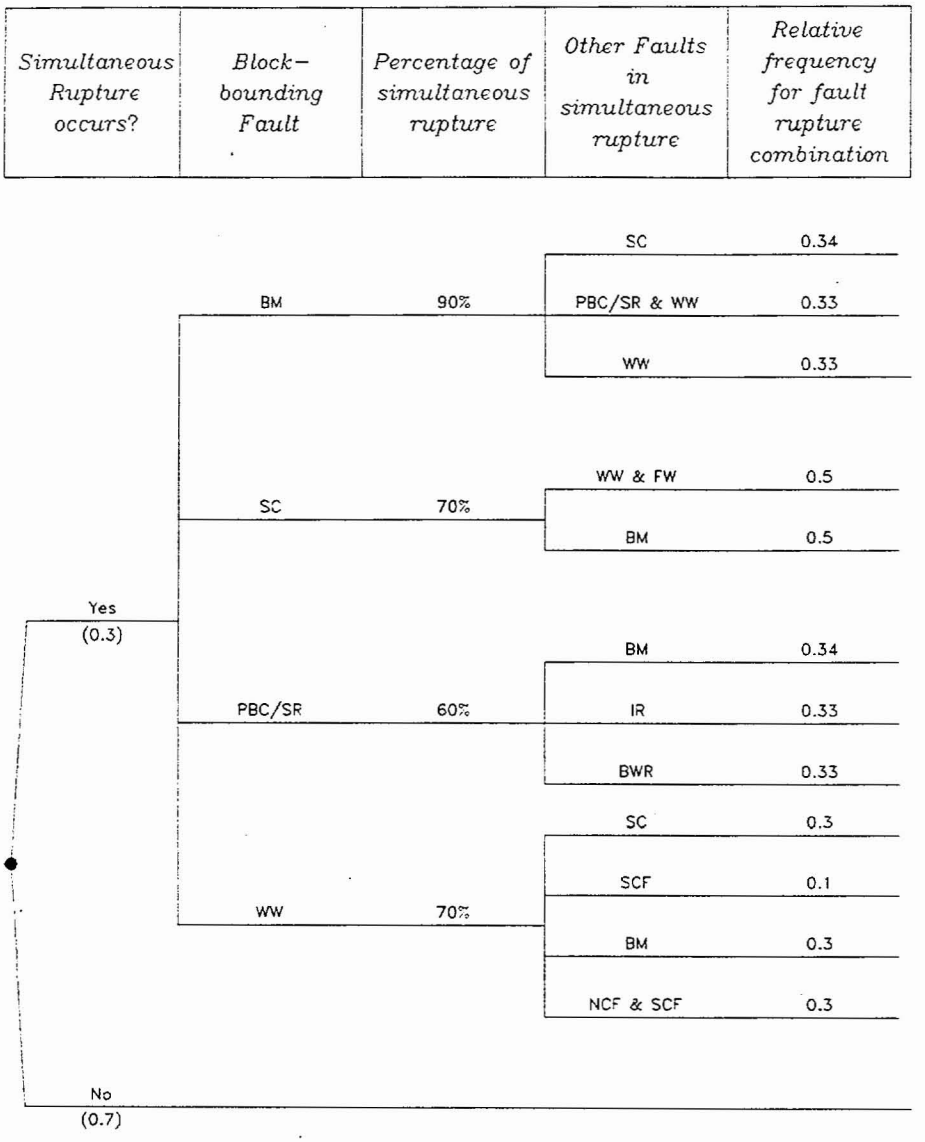

Explanation:

BM – Bare Mountain
SC – Solitario Canyon
PBC/SR – Paintbrush Canyon/Stagecoach Road
WW – Windy Wash
FW – Fatigue Wash
IR – Iron Ridge
BWR – Bow Ridge
SCF – South Crater Flat
NCF – North Crater Flat

Figure ASM-8 Simultaneous rupture scenarios and relative frequencies

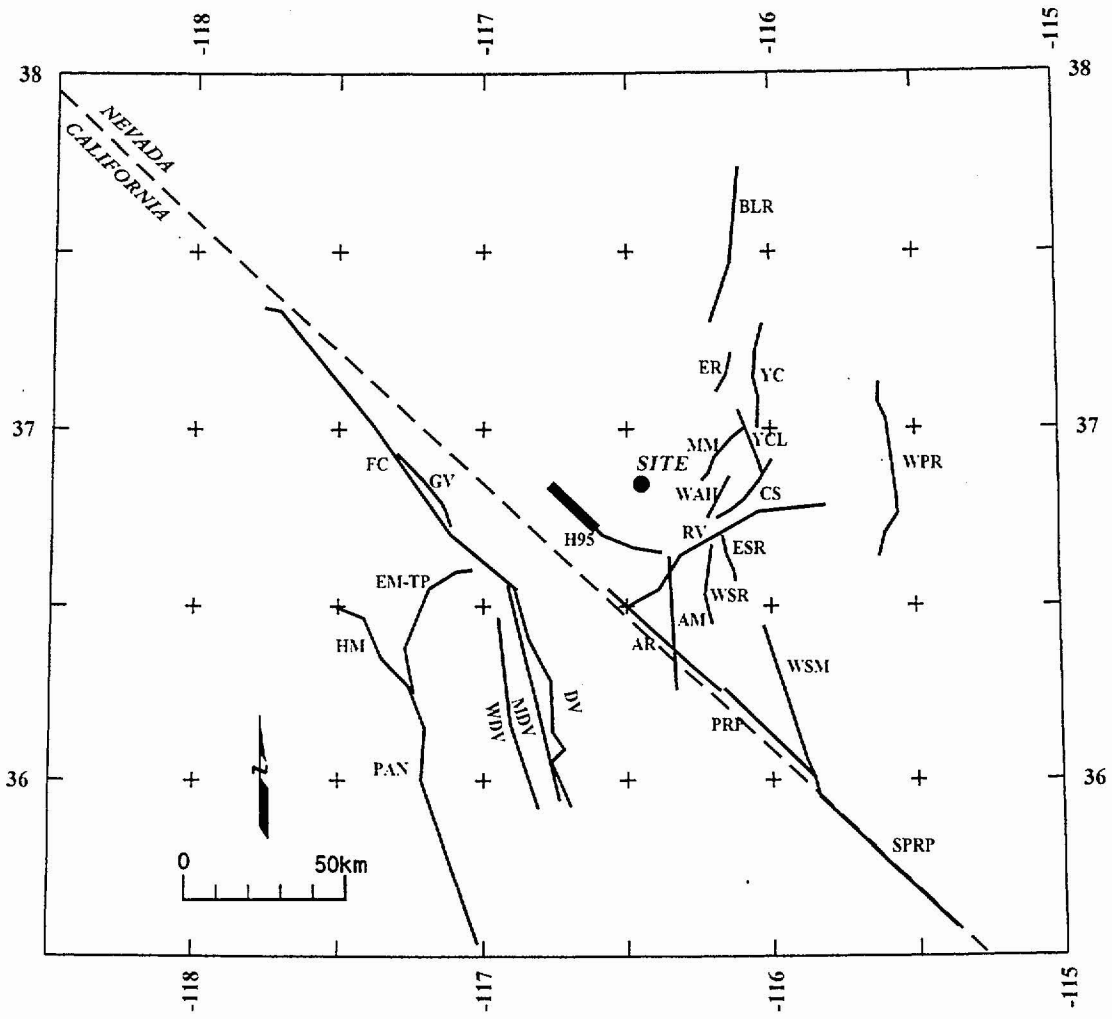

EXPLANATION

NOTE: Fault names are listed in Table ASM-6

Fault Lengths:

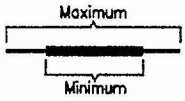

Figure ASM- 9 Map showing regional faults included in the seismic source model

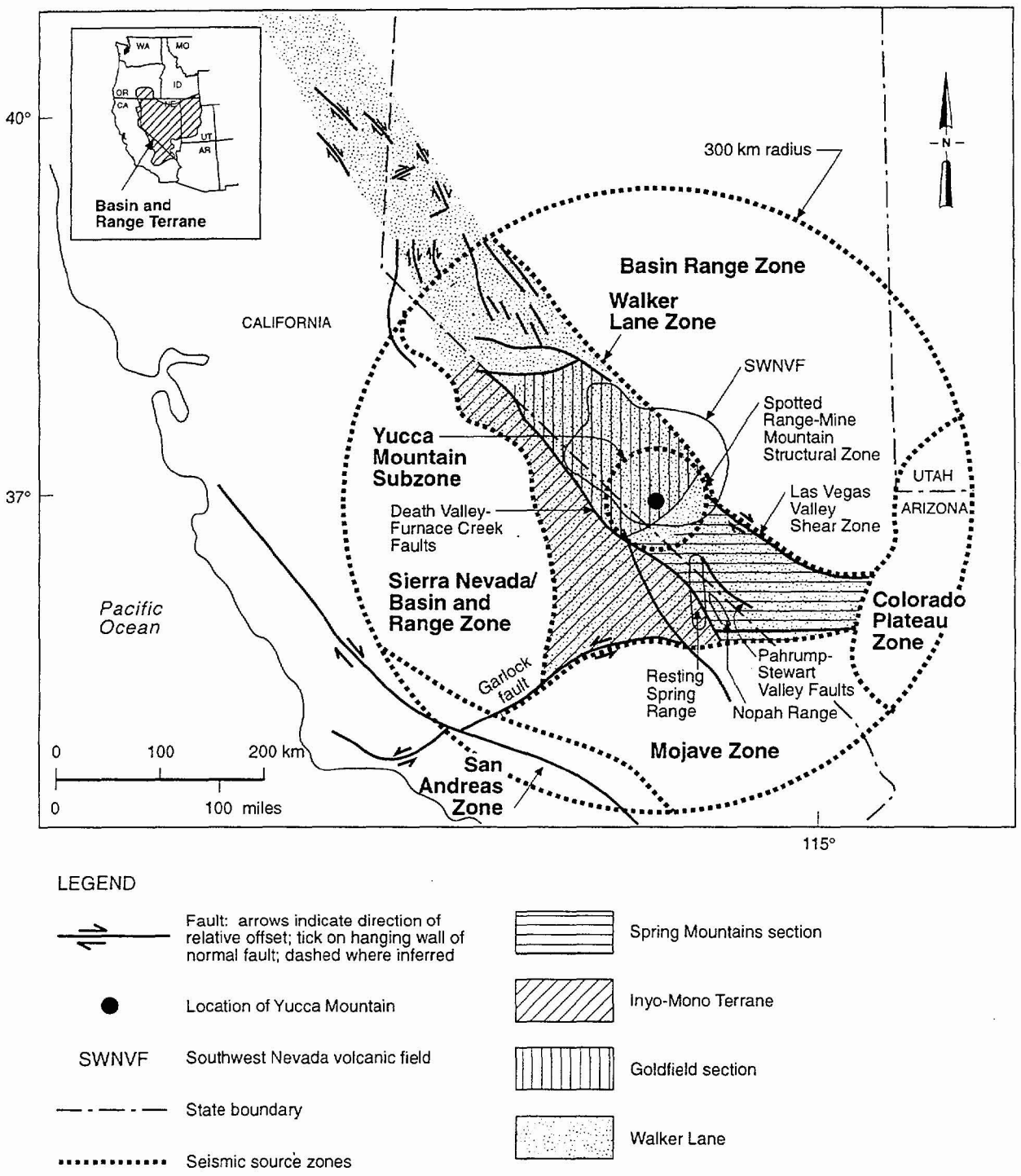

Figure ASM-10 Map of regional seismic source zones within 300 km

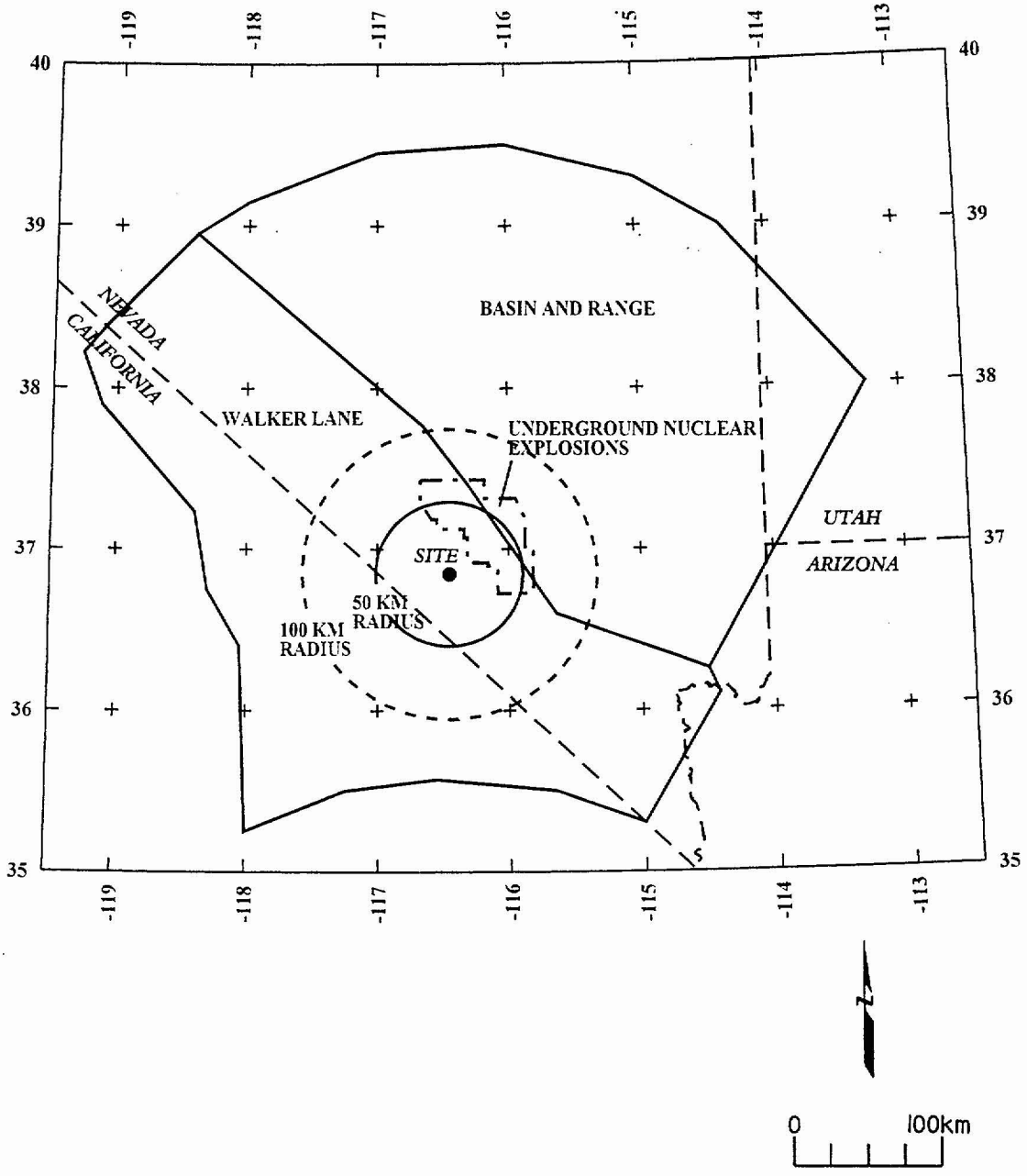

Figure ASM-11 Map showing the boundaries of zones used in the seismic source model

h:\prj\yucca_mt\dgn\1097\plate_ti_reg_zone.dgn 27-OCT-1997 14:26

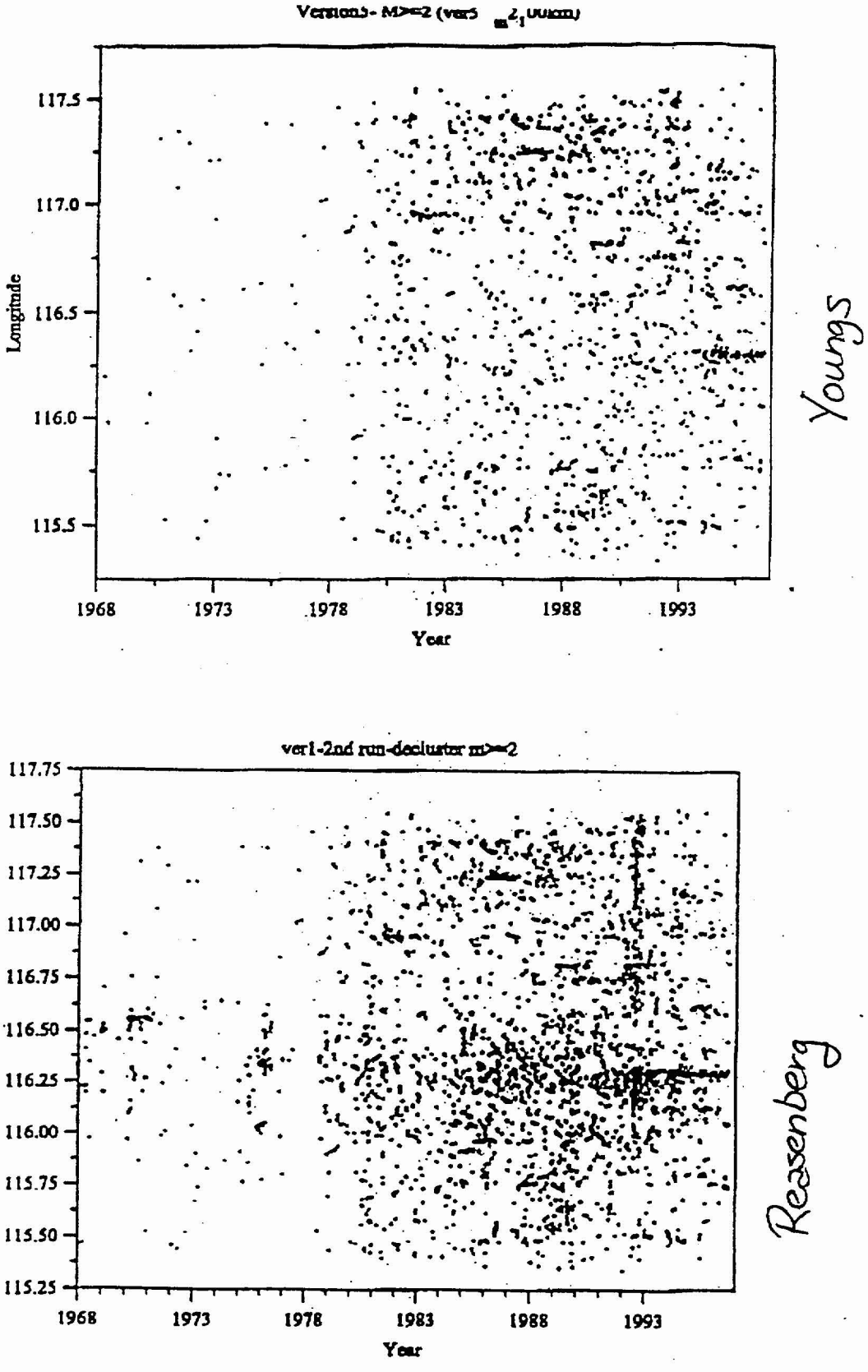

Figure ASM-12 Space-time diagrams comparing Youngs and Reasenberg declustering methods

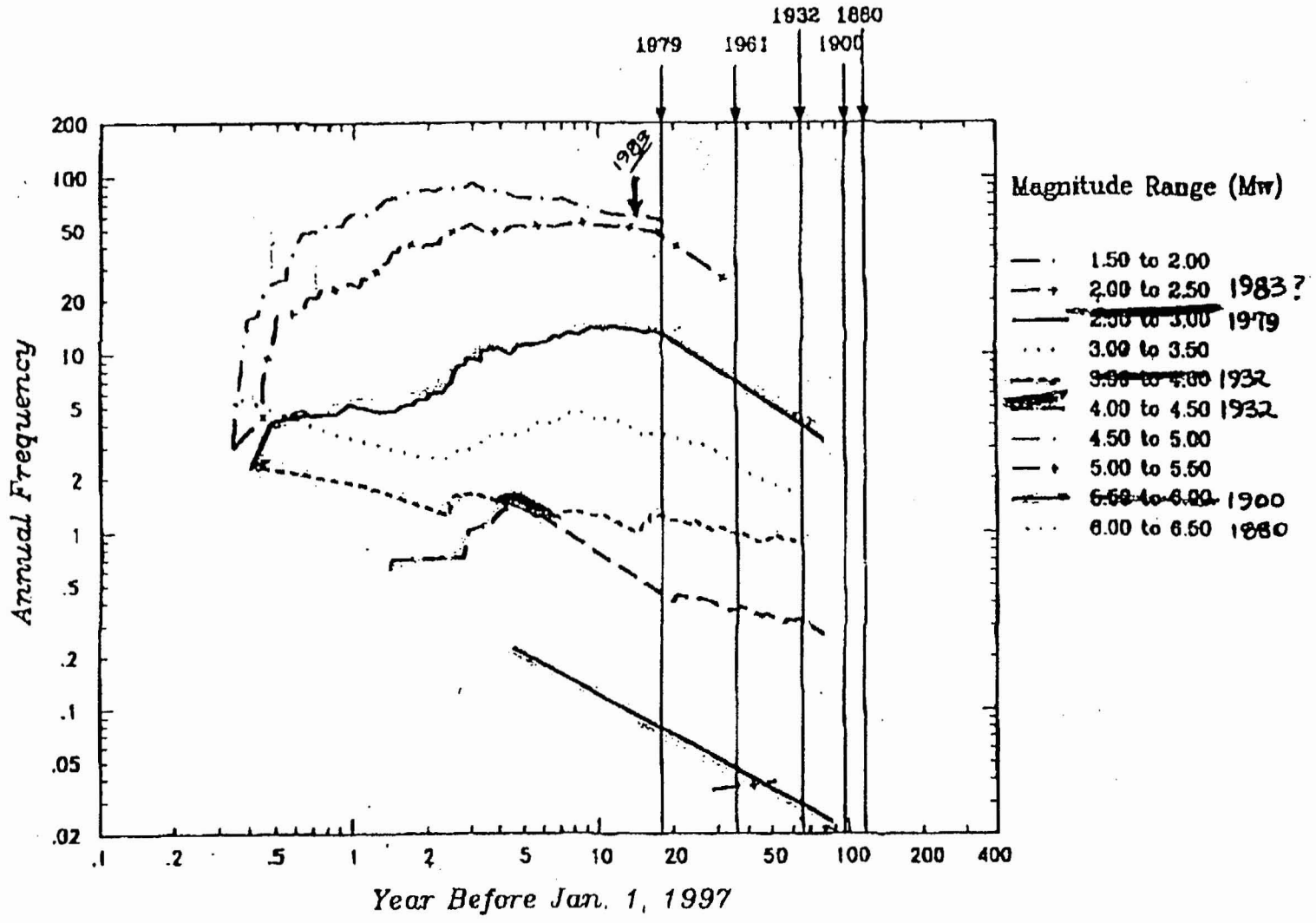

Figure ASM-13 Annual frequency of earthquake recurrence as a function of time before Jan. 1, 1997, based on the catalog declustered by approach of Youngs et al.

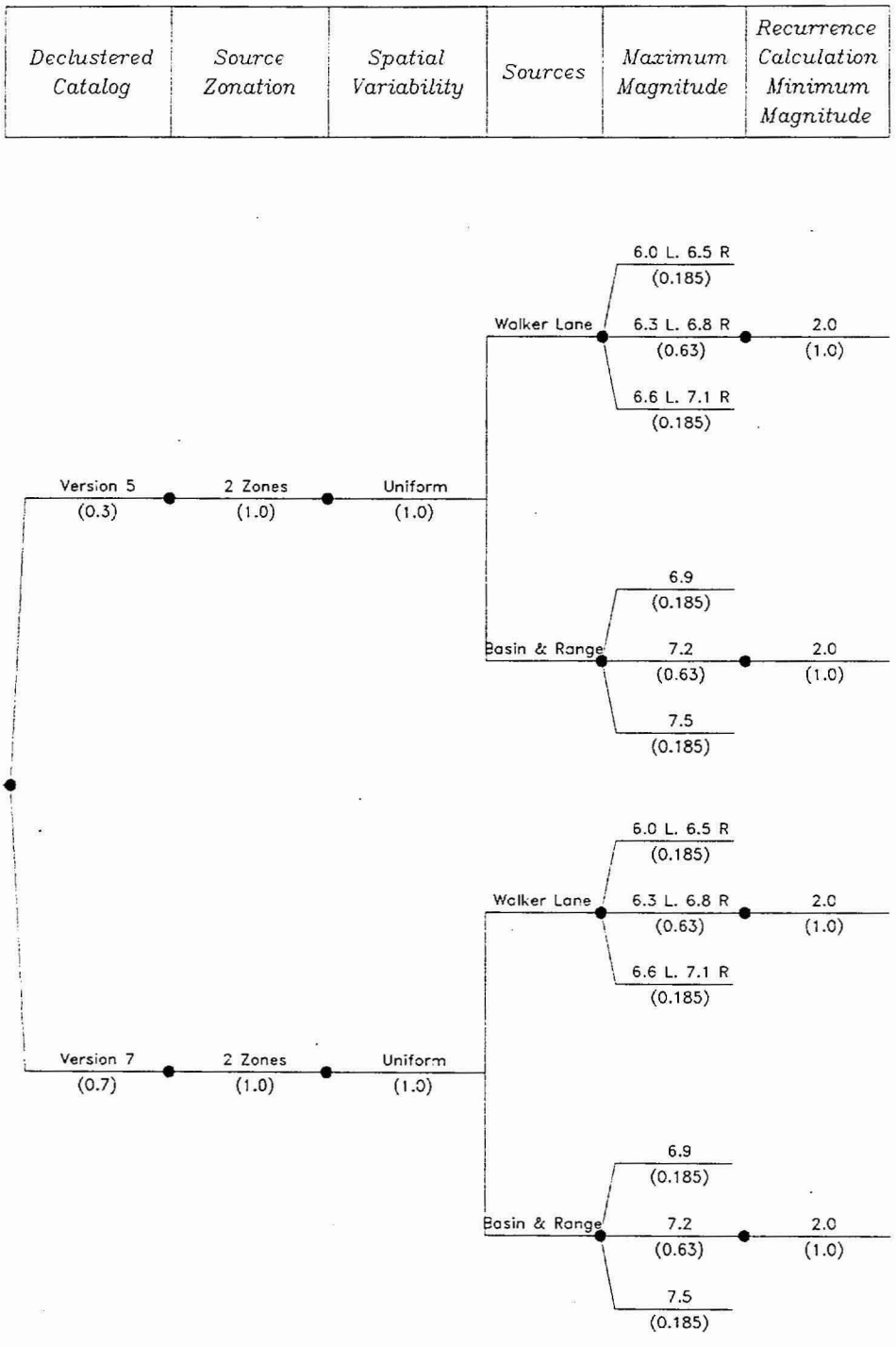

Figure ASM-14 Logic tree used to characterize seismic source zones

Principal Faulting Capability	*Earthquake Frequency*	*Probability of Surface Rupture*	*Maximum Displacement*	*Displacement Distribution*

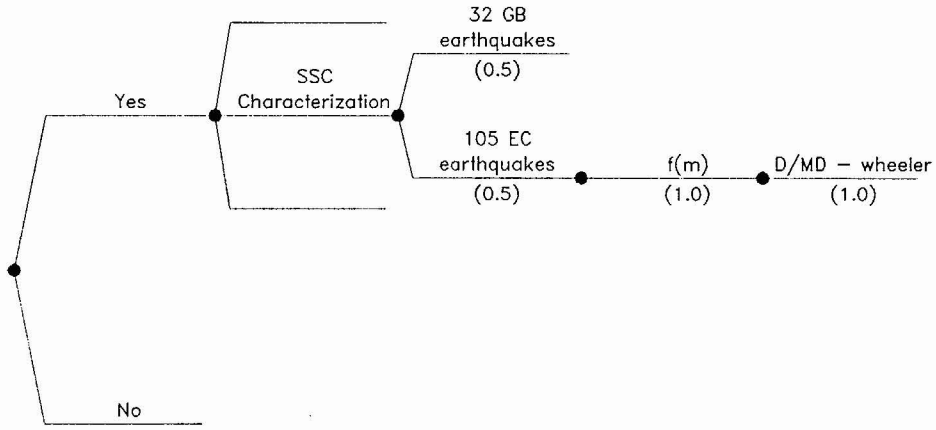

Figure ASM-16a Logic tree for principal faulting hazard

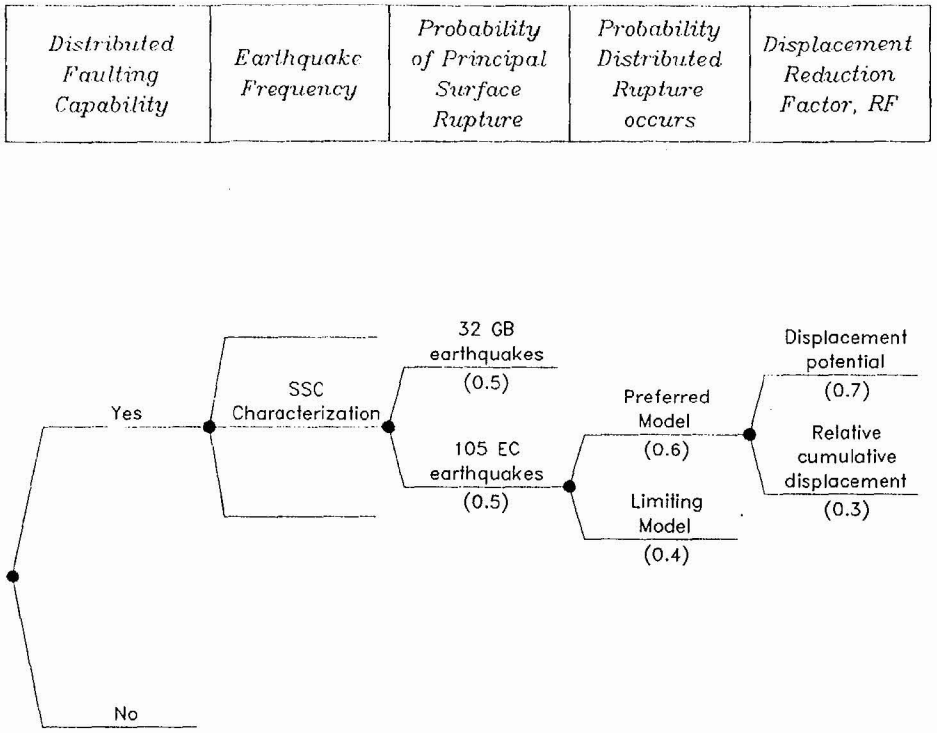

Figure ASM-16b Logic tree for distributed faulting hazard

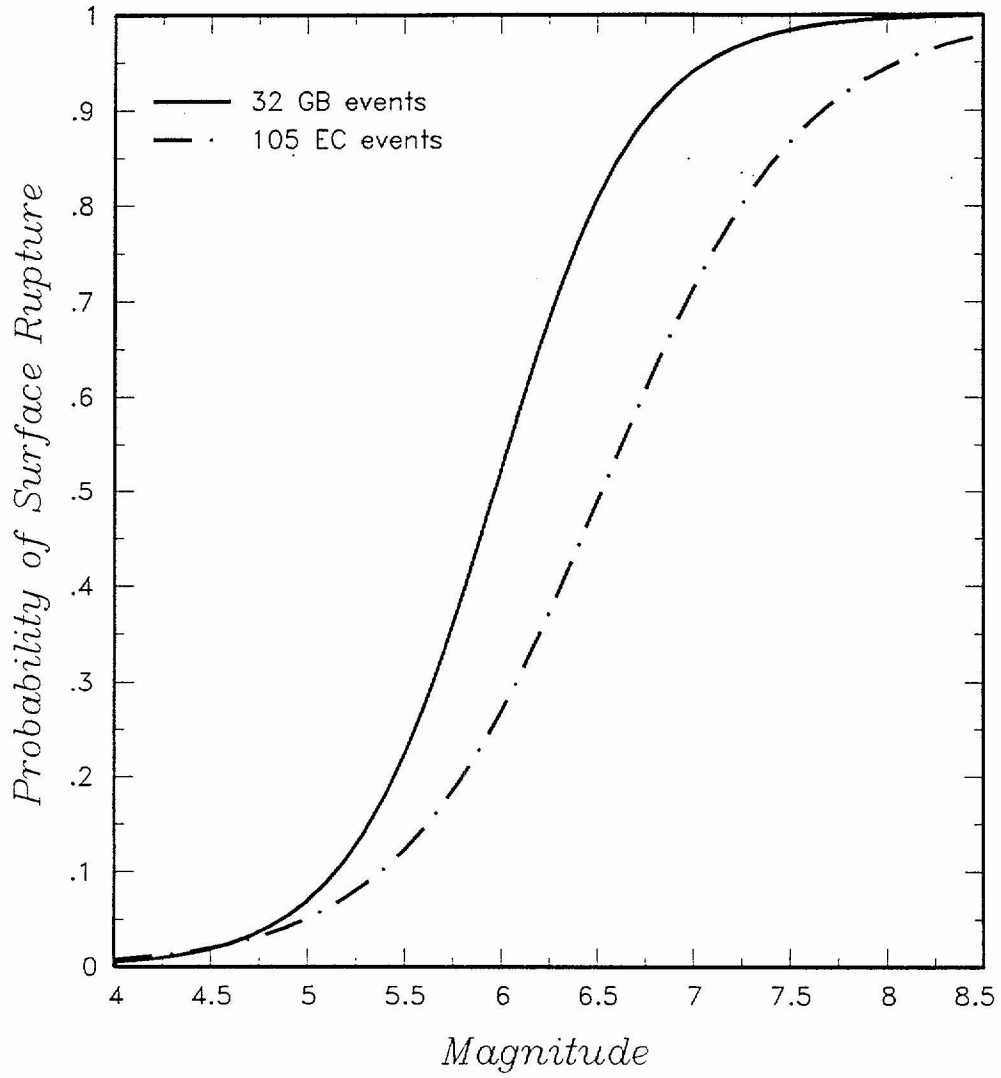

Figure ASM-17 Relationships between earthquake magnitude and probability of surface rupture

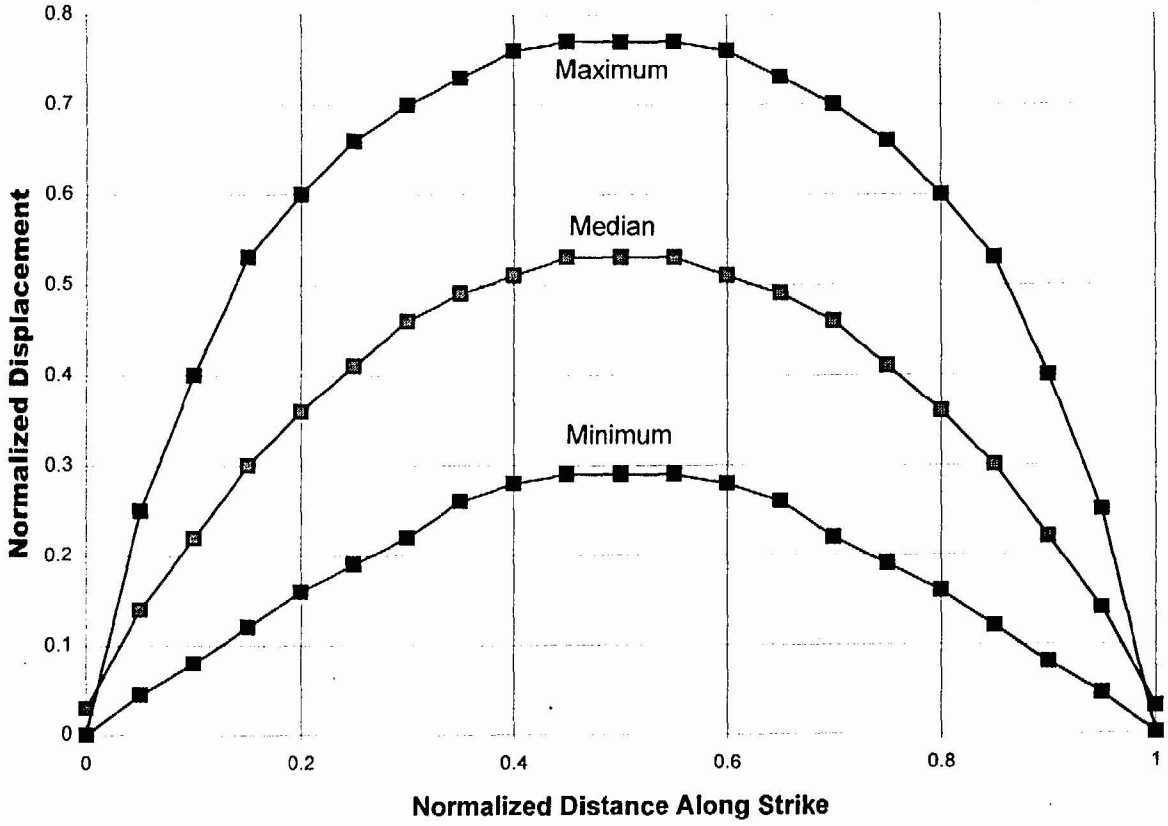

Figure ASM-18 Normalized "Wheeler" curve (adapted from Wheeler, 1989)

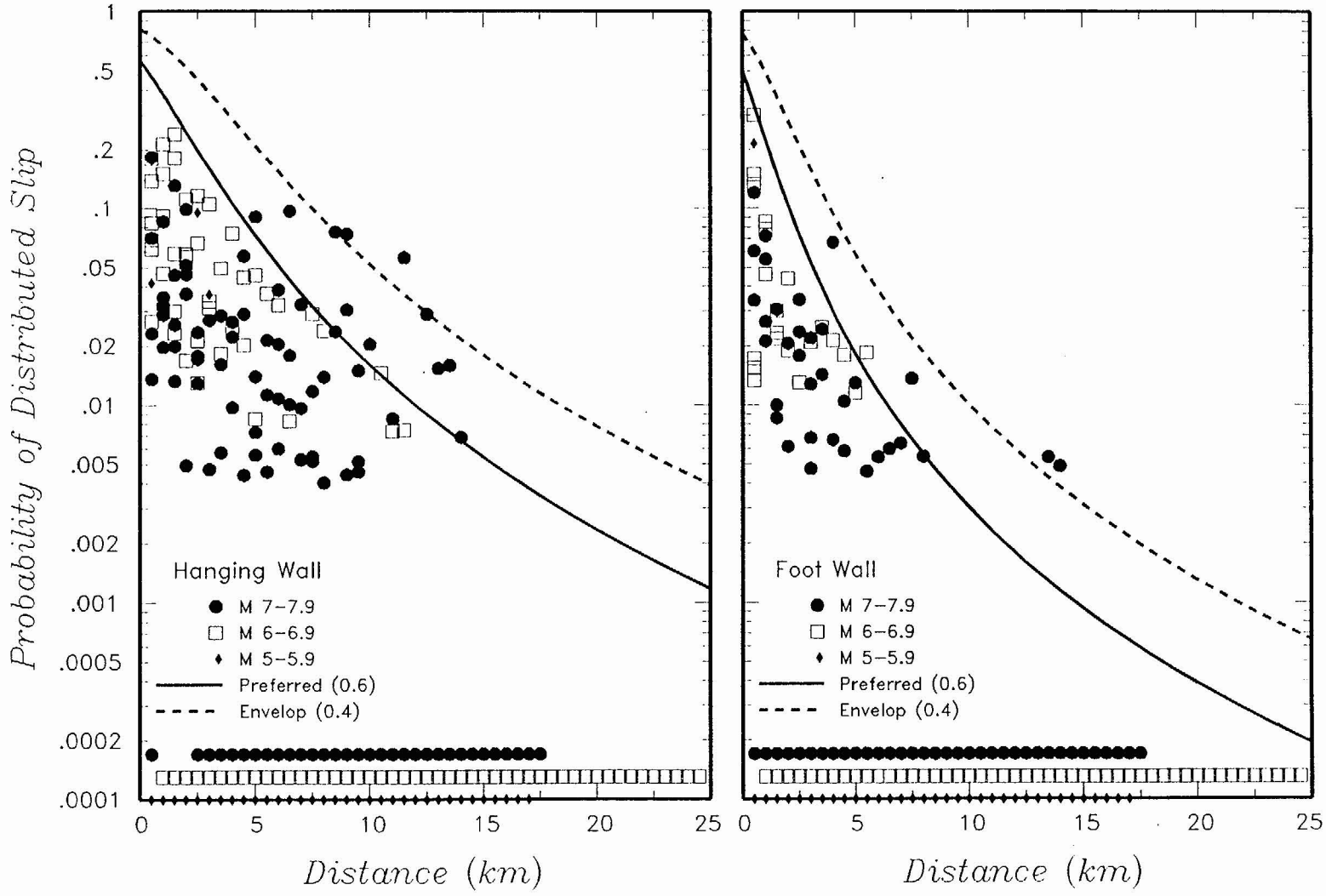

Figure ASM-19 Probability (frequency) of distributed slip as a function of distance from rupture

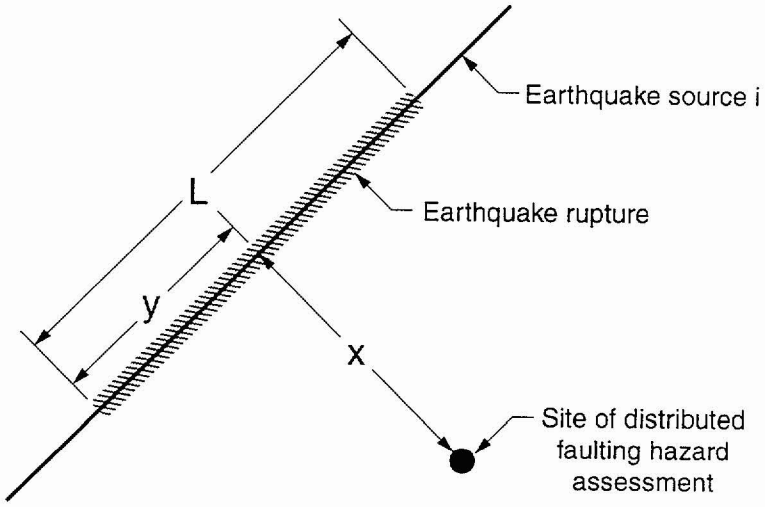

x = distance from rupture to site measured from fault normal point

y = location of fault normal point within rupture

L = length of earthquake rupture

Figure ASM-20 Schematic illustration of ASSD method

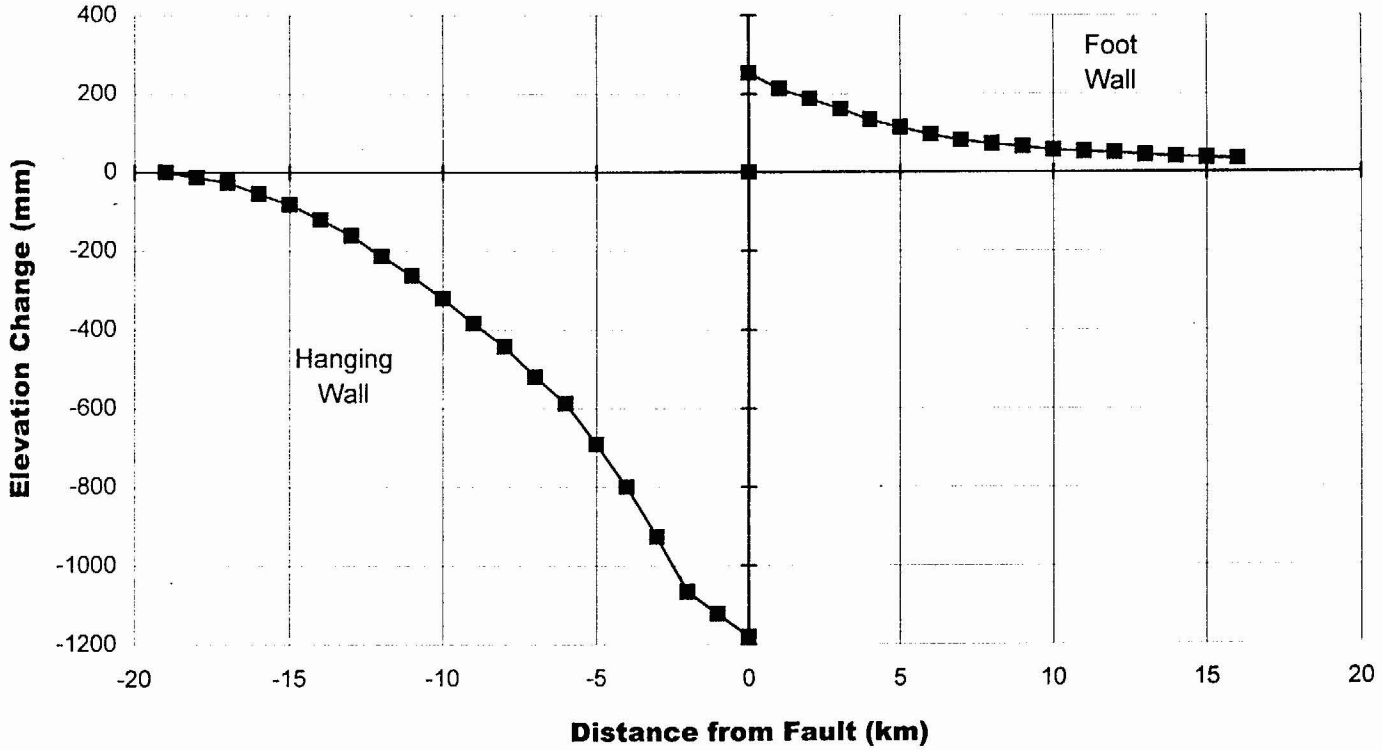

Figure ASM-21 Borah Peak geodetic curve

APPENDIX ASM-1

Graphs showing the cumulative frequency of long-term slip rates for 10 local Yucca Mountain faults.

Note: These CDFs were computed from permutations of cumulative displacement and age of deposits/soils from Table 5-1 in USGS (written communication, 1996).

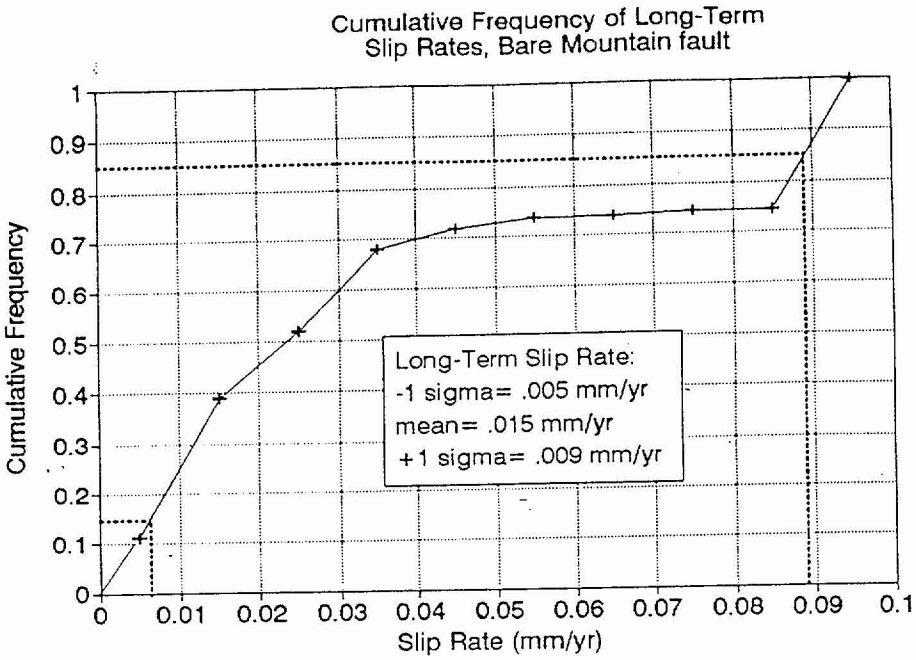
Cumulative Frequency of Long-Term Slip Rates, Bare Mountain fault
Cumulative Frequency
Slip Rate (mm/yr)
Long-Term Slip Rate:
-1 sigma= .005 mm/yr
mean= .015 mm/yr
+1 sigma= .009 mm/yr
0
0.1
0.2
0.3
0.4
0.5
0.6
0.7
0.8
0.9
1
0.01
0.02
0.03
0.04
0.05
0.06
0.07
0.08
0.09
0.1

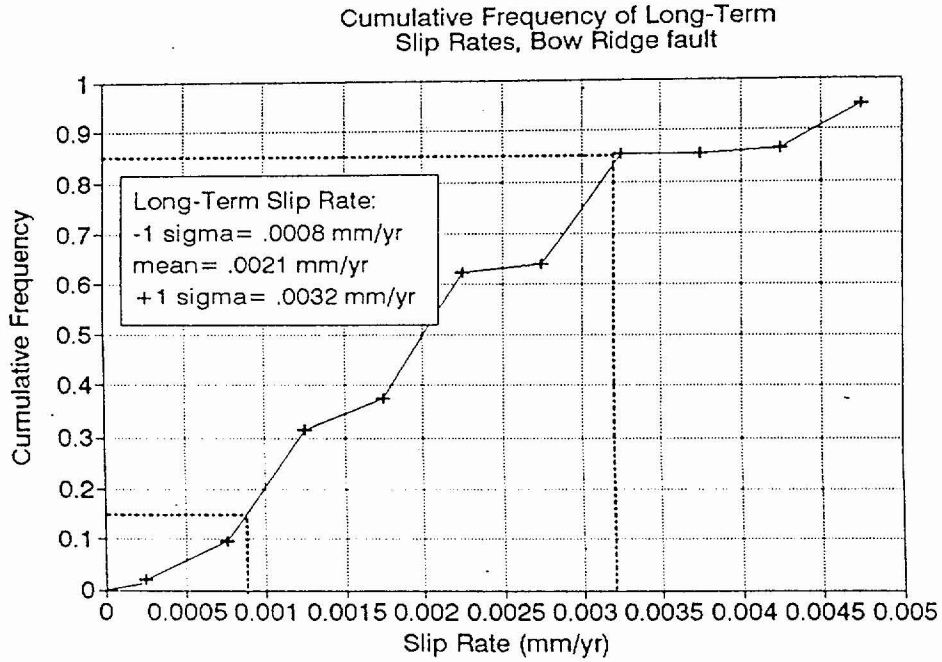
Cumulative Frequency of Long-Term Slip Rates, Bow Ridge fault
Cumulative Frequency
Slip Rate (mm/yr)
Long-Term Slip Rate:
-1 sigma= .0008 mm/yr
mean= .0021 mm/yr
+1 sigma= .0032 mm/yr
0
0.1
0.2
0.3
0.4
0.5
0.6
0.7
0.8
0.9
1
0.0005
0.001
0.0015
0.002
0.0025
0.003
0.0035
0.004
0.0045
0.005

ASM-AI-2